Frontiers in Bioscience Landmark

Front. Biosci. (Landmark Ed) **2026**; 31(1): 46605
https://doi.org/10.31083/FBL46605

Original Research

TGF-β/RhoA/ROCK Signaling Activation Orchestrates Ciliary Body EMT and Fibrosis in Myopia

Xuewei Yin[1,2,3,†], Yixian Hao[2,†], Zhongyu Ma[1], Yunxiao Xie[2], Bo Bao[1], Huixia Wei[2], Qiuxin Wu[2], Tuling Li[1], Jiawen Hao[1], Xuan Zhang[1], Hongsheng Bi[2,3], Dadong Guo[1,3,4,*]

[1]School of Ophthalmology and Optometry, Shandong University of Traditional Chinese Medicine, 250002 Jinan, Shandong, China
[2]Affiliated Eye Hospital of Shandong University of Traditional Chinese Medicine, 250002 Jinan, Shandong, China
[3]Shandong Provincial Key Laboratory of Integrated Traditional Chinese and Western Medicine for Prevention and Therapy of Ocular Diseases, 250002 Jinan, Shandong, China
[4]Shandong Academy of Eye Disease Prevention and Therapy, 250002 Jinan, Shandong, China
*Correspondence: dadonggene@sdutcm.edu.cn (Dadong Guo)
[†]These authors contributed equally.

Academic Editor: Dario Rusciano
Submitted: 15 September 2025 Revised: 20 November 2025 Accepted: 16 December 2025 Published: 16 January 2026

Abstract

Background: Dysregulation of the transforming growth factor (TGF)-β/Ras homolog family member A (RhoA)/Rho-associated protein kinase (ROCK) pathway can lead to fibrotic changes in ocular diseases. The present study investigated its role in epithelial–mesenchymal transition (EMT) and fibrosis in the ciliary body in lens-induced myopia (LIM) guinea pigs. **Methods**: A lens-induced myopia model was established in guinea pigs. Refraction, axial length, and ciliary body alterations were assessed via quantitative polymerase chain reaction (qPCR), western blot, PCR array, histological, and biomechanical analyses. Upstream mechanisms were explored using Ingenuity Pathway Analysis. Functional experiments were performed using the ROCK inhibitor Y-27632. **Results**: Refraction and axial length were increased in the myopic ciliary body in a time-dependent manner. Protein levels of TGF-β1, RhoA, ROCK1, ROCK2, α-smooth muscle actin (α-SMA), and matrix metalloproteinase (MMP)1 were significantly elevated in the myopic ciliary body, peaking at 6 weeks. In the ultra-early stage of lens myopia, functional changes such as refractive errors and increased biological parameters like axial length occur earlier than changes in EMT transcription factor levels. The differentially expressed genes were involved in cell movement, development, growth, proliferation, and transport in early myopia. Compared with those of normal animals, the Ca^{2+} inflow and Young's modulus of the ciliary body were greater, the ciliary body elasticity was lower, and the degree of tissue fibrosis was aggravated in animals with deepening myopia. Furthermore, ROCK inhibition can alleviate the pathological levels of EMT and fibrosis in the cilia of myopic guinea pigs. **Conclusion**: Collectively, our findings indicate that activation of the TGF-β/RhoA/ROCK pathway induces EMT in the ciliary body, promotes Ca^{2+} inflow, and reduces ciliary body elasticity in myopic animals, resulting in tissue fibrosis and dysfunction. It provides a new perspective on the pathological mechanisms of ciliary body fibrosis in the development of myopia.

Keywords: myopia; ciliary body; TGF-β/RhoA/ROCK signaling; EMT; fibrosis

1. Introduction

Myopia has become a global public health problem. In East Asia and Southeast Asia, the prevalence of myopia among adolescents is approximately 80–90%, and the prevalence of high myopia is 10–20% [1,2]. In addition, high myopia ($\geq$–6.0 D) can lead to severe complications such as irreversible vision loss, retinal detachment, cataracts, and macular atrophy [3]. A survey conducted among children aged 5–15 years in China found that the prevalence of myopia gradually increases with age, from 5.7% at the age of 5 years to 30.1% at the age of 10 years and 78.4% at the age of 15 years [4]. Therefore, exploring the pathogenesis of myopia and discovering new targets for the clinical treatment of myopia are highly important.

Close work aggravates myopia progression, and it is hypothesized that more accommodation is produced to stimulate eyeball growth during close work [5]. Studies have shown that the ciliary muscle of children with myopia increases abnormally, indicating that the development of myopia may be related to the ciliary muscle [6]. In addition, myopia is usually accompanied by accommodation lag, and abnormalities in the ciliary muscle may be the source of accommodation lag, resulting in retinal defocus and axial elongation of the eyeball [7,8]. Therefore, the ciliary muscle plays an essential role in the progression of myopia, although the exact mechanisms remain unclear.

As smooth muscle, the ciliary muscle comprises mainly muscle fiber bundles, and type I collagen (Col-1), Col-3, and fibronectin (FN) are present in the connective tissue between muscle bundles [9]. Moreover, matrix metalloproteinases (MMPs) 1, 2, 3, 11, 12, 14, 15, 16, 17, 19, and 24, as well as tissue inhibitors of metalloproteinases

(TIMPs) in the ciliary muscle, are also widely expressed. Many studies have shown that the Ras homolog family member A (RhoA)/Rho-associated protein kinase (ROCK) signaling pathway is involved in regulating cell proliferation and differentiation, which induces cytoskeleton reorganization, thus affecting vascular permeability, tissue permeability, and stress fiber formation. Fibrosis can occur in multiple organs of the body and is characterized mainly by hyperplasia of fibrous connective tissue and a reduction in parenchymal cells [10,11]. Under the influence of certain pathological factors, the fibrotic response can occur in intraocular tissues, such as corneal fibrosis, conjunctival fibrosis, retinal fibrosis, and scleral fibrosis [12–14]. During the development of fibrosis, fibrosis manifests mainly as extracellular matrix (ECM) deposition and excessive generation of mesenchymal stromal cells (such as fibroblasts and myofibroblasts), among which the activation of fibroblasts plays an important role in the development of fibrosis [15]. In fibrotic tissues, interstitial fibroblasts can be transformed into myofibroblasts, which further accumulate and secrete excessive collagen, eventually forming a fibrotic collagen network [16].

Additionally, dedifferentiated epithelial cells acquire mesenchymal markers, which transform them into mesenchymal, stromal-like cells. A significant portion of myofibroblasts during fibrosis are derived from fibroblasts transformed by epithelial-mesenchymal transition (EMT) of epithelial cells [17]. Key regulators of the EMT process include the Snail family transcription factors (Snail1 and Slug), the Twist family transcription factors (Twist1 and Twist2), and the transcription factor zinc finger E-box binding protein 1(Zeb1). An increase in the expression levels of these transcription factors facilitates the occurrence of EMT. EMT is the process by which epithelial cells differentiate into mesenchymal cells. EMT is involved in development, wound healing, and stem cell behavior, and it contributes to the development of fibrosis.

Additionally, transforming growth factor (TGF)-β family signaling plays a dominant role in reprogramming gene expression and in nontranscriptional changes during EMT [18]. TGF-β is involved in the development of fibrosis, mainly by regulating ECM deposition and reducing ECM degradation by inhibiting the activity of MMPs [19]. TGF-β1 induces the activation of the Rho-associated protein kinase (ROCK) signaling pathway and regulates the expression of α-smooth muscle actin (α-SMA) and Col I [20]. Therefore, the TGF-β/RhoA/ROCK signaling pathway may affect the ciliary body morphology and ECM deposition to induce ciliary body fibrosis, leading to dysfunction of the ciliary body and ultimately myopia progression. Currently, the EMT and fibrosis of the ciliary body have not been studied in experimental myopia guinea pig models. This study aimed to delineate the alterations in ciliary body morphology and biomechanical properties during myopia, utilizing a –6.0 D lens-induced guinea pig model of myopia (LIM). The expression levels of TGF-β1, RhoA, ROCK1/2, α-SMA, and MMP-1 in LIM guinea pig ciliary body were investigated. The present research will facilitate a better understanding of the changes in the ciliary body microenvironment during myopia progression, providing new insights into the pathogenesis of myopia.

2. Materials and Methods

2.1 Animals and Groups

The present study was approved by the Ethics Committee of the Affiliated Hospital of Shandong University of Traditional Chinese Medicine (AWE-2022-055). All the animal studies were performed in strict accordance with the ARVO Statement for the Use of Animals in Ophthalmic and Vision Research. Three-color short-haired healthy guinea pigs (2 weeks old, male, and 110–130 g) were supplied by Danyang Changyi Experimental Animal Breeding Co., Ltd. In an animal room with a constant temperature of 20–25 °C, all animals were reared in clean, transparent plastic cages (5–6 per cage) under 300 lux light for a 12/12 h day and night cycle, with feeding conditions. Before enrollment, all experimental animals received ocular examination by a computerized refractometer (TOPCON, KR8900, Japan) and a hand-held retinal camera (Japan Kowa Co., Ltd., Genesis-D) to eliminate spontaneous myopia, cataracts, or corneal disease. After a 1-week adaptive feeding period, the study cohort of 120 healthy guinea pigs underwent randomization into the normal control (NC) and LIM group, 1-week (n = 40), 2-week (n = 40), and 6-week (n = 40) subgroups according to the duration of myopia induction. To induce LIM, –6.0 D lenses were placed on the right eyes of guinea pigs in the LIM group, while the left eyes, which received no treatment, served as self-controls. The lenses were kept clean throughout the duration of myopia progression, and the guinea pigs in the NC group received no intervention. In addition, functional verification experiments were conducted using the ROCK inhibitor Y-27632 (SJ-MX1027A, Shandong SparkJade Biotechnology Co., Ltd., Jinan, China). In the Y27632 group of myopic guinea pigs, Y27632 was administered as eye drops to the right eye three times a day at a concentration of 10 mM.

2.2 Measurement of Diopter and Axial Length

The diopter of the guinea pigs was evaluated before enrollment and after 1 week, 2 weeks, and 6 weeks of myopia induction. Prior to the examination, 10 g·L^{-1} cyclopentolate hydrochloride eye drops (Alcon, USA) were instilled into the conjunctival sac once every 5 min for a total of 3 times. After the pupil was in a state of complete divergence, a strip retinoscope (Liu Liu Vision Technology Co., Ltd., YZ24, Suzhou, China) was used for binocular diopter detection. The diopter value was obtained from the average of the vertical and horizontal meridians. The ocular axial length was measured by the ophthalmic A-scan

ultrasonography (Cinescan, Quantel Medical, France). The instrument parameters were as follows [21]: the propagation velocity of the anterior chamber was 1557 $m \cdot s^{-1}$, the propagation velocity of the vitreous body was 1540 $m \cdot s^{-1}$, and the propagation velocity of the lens was 1723 $m \cdot s^{-1}$. Before the measurements, the guinea pigs in each group were anesthetized with 4 $mg \cdot mL^{-1}$ Obukaine hydrochloride eye drops (Santen Pharmaceutical Co., Ltd., Japan), and the probe was then gently touched to the cornea to measure the axial length. The average value of 10 continuous measurements represented the final axial length of the guinea pig. All the above measurements of diopter and axial length were conducted by the same inspector under the same operating standards. All experiments were independently repeated at least three times, and all measurement data are presented as means ± SEM (n = 30).

2.3 Ciliary Body Isolation

After 1, 2, and 6 weeks of myopia induction, the guinea pigs in each group were anesthetized by intraperitoneal injection of 3% pentobarbital sodium (30 mg/kg), and the right eyeballs were removed. The ciliary body tissue was then isolated under a microscope. The ciliary body tissue was washed in 1× PBS rinse solution (CR0014, SparkJade, China), placed in cryogenic vials (NEST Biotech, Wuxi, China), weighed, quickly frozen in liquid nitrogen, and stored at –80 °C. The guinea pigs were euthanized by an additional intraperitoneal injection of pentobarbital sodium (200 mg/kg) to achieve excessive anesthesia.

2.4 Real-Time Quantitative Polymerase Chain Reaction (RT-qPCR)

At the indicated times, the ciliary bodies of guinea pigs were randomly isolated, and total RNA was isolated with a modified SPARKeasy tissue/cell RNA extraction kit (AC0202-B, SparkJade, Jinan, China). Some of these RNA samples were also used for subsequent RT^2 Profiler™ PCR Array detection. After the transcription of cDNA, the expression levels of the *TGF-β1*, *RhoA*, *ROCK1*, *ROCK2*, *α-SMA*, *MMP1*, *Snail1*, *Slug*, *Twist1*, *Twist2*, and *Zeb1* genes in the ciliary body were detected by RT-qPCR. The primer sequences are listed in Table 1, and the specificity of the RT-qPCR product was confirmed by melting curve analysis. The following PCR cycling program was used: 30 s at 95 °C; 45 cycles of 10 s at 95 °C and 10 s at 62 °C. All experiments were independently repeated at least three times, and these RT-qPCR data are presented as means ± standard error of the mean (SEM) (n = 6). To quantify relative gene expressions in the ciliary body, transcript levels were normalized to the housekeeping gene Glyceraldehyde-3-phosphate dehydrogenase (*GAPDH*) and calculated via the $2^{-\Delta\Delta CT}$ method.

Table 1. Primer sequences of Q-PCR reaction.

Gene	Primer sequences
GAPDH	F: 5′-CTGACCTGCCGCCTGGAGAAACC-3′
	R: 5′-ATGCCAGCCCCAGCGTCAAAAGT-3′
TGF-β1	F: 5′-AACCGGCCCTTCCTGCTCCTCAT-3′
	R: 5′-CGCCGGGGTTGTGCTGGTTGTA-3′
RhoA	F: 5′-TTTCTGTCCCAACGTACCCATTAT-3′
	R: 5′-ACAAGACAAGGCACCCAGATTTTT-3′
ROCK1	F: 5′-ATGAAGGGGAATGTAGAAAAGACG-3′
	R: 5′-TTGGCAGGAAAGTGGTAGAGTGTA-3′
ROCK2	F: 5′-CGAGGCCGAGCAGTATTTCT-3′
	R: 5′-TCGGCGAGCTCCTGTTTGTG-3′
α-SMA	F: 5′-CCGGCTTTGCTGGGGACGAT-3′
	R: 5′-CCGGTTGGCCTTGGGATTGAG-3′
MMP1	F: 5′-CAGAGGAGAACACGGTGACAATAA-3′
	R: 5′-CATGAGCCGCAGAATAATACAAGT-3′
Snail1	F: 5′-ATGCCGCGCTCGTTCCTTGTCA-3′
	R: 5′-GCCCTTCCCGCTGTCCTCGTCA-3′
Slug (Snail2)	F: 5′-TGCCGCGCTCCTTCCTG-3′
	R: 5′-ATGGTAATGGGGCTGTATGCTC-3′
Twist1	F: 5′-GCAGGGCAAGCGCGGCAAAAA-3′
	R: 5′-CCGAGGGCAGAGTGGGGATGAT-3′
Twist2	F: 5′-CGGGCAAGCGCGGCAAGAA-3′
	R: 5′-CGAGGGCAGCGTGGGGATGAT-3′
Zeb1	F: 5′-CACAGTCTGGGGGTAATCGTAAAT-3′
	R: 5′-TTGTGGCCGGGTGGGACTG-3′

GAPDH, Glyceraldehyde-3-phosphate dehydrogenase; *TGF*, transforming growth factor; *RhoA*, Ras homolog family member A; *ROCK*, Rho-associated protein kinase; *α-SMA*, α-smooth muscle actin; *MMP*, matrix metalloproteinase; *Snail* (*Slug*), Snail family transcriptional repressor; *Twist*, Twist transcription factor; *Zeb1*, zinc finger E-box binding protein 1.

2.5 Western Blot Analysis

At the indicated times, the ciliary body tissues of the right eye of the guinea pigs in each group were separated (n = 6), and total protein was extracted with radioimmunoprecipitation assay (RIPA) lysis buffer (EA0002, Sparkjade, China) containing phenylmethylsulfonyl fluoride (PMSF) (EA0005, Sparkjade, China). After homogenization and sonication, the lysed tissues were centrifuged at 5000 ×g for 5 min, and the supernatants were collected. The concentration of total protein was measured with an enhanced BCA protein concentration assay kit (P0010, Beyotime, Shanghai, China) in a 96-well plate (NEST Biotech., Wuxi, China). The proteins were separated on 10% sodium dodecyl sulfate (SDS)-polyacrylamide gel electrophoresis (PAGE) gels (EC1023-B, SparkJade, China) and then transferred to a polyvinylidene fluoride (PVDF) membrane. The PVDF membrane was subsequently blocked with 5% nonfat milk solution for 1.5 h. After blocking, the PVDF membrane was incubated at 4 °C overnight with the primary antibody mixture (dilution ratio = 1:1000, ED0013) (Table 2). The PVDF membrane was then incubated with goat anti-

Table 2. Primary antibody reagents.

Name	Source
Rabbit Anti-TGF beta1 (bs-0086R)	Bioss Biotechnology Co., Ltd., Beijing
RhoA Rabbit pAb (A13947)	Wuhan Aibotech Biotechnology Co., Ltd.
Rabbit Anti-ROCK1 (bs-1166R)	Bioss Biotechnology Co., Ltd., Beijing
Rabbit Anti-ROCK2 (bs-1205R)	Bioss Biotechnology Co., Ltd., Beijing
Rabbit Anti-alpha smooth muscle Actin (bs-0189R)	Bioss Biotechnology Co., Ltd., Beijing
Rabbit Anti-MMP-1 (bs-4597R)	Bioss Biotechnology Co., Ltd., Beijing
Rabbit Anti- E-Cadherin (F0005)	Selleck Biotechnology Co., Ltd., USA
Anti-N-Cadherin Rabbit pAb (WL01047)	Wanleibio Co., Ltd., Shenyang
β-Actin Rabbit mAb (High Dilution) (AC026)	Wuhan Aibotech Biotechnology Co., Ltd.

rabbit IgG (H+L) HRP (EF0002, SparkJade, China) diluent (dilution ratio = 1:5000) for 1 hour. Finally, the FUSION FX multifunction imaging system (Vilber Lourmat, Marne-la-Vallée, France) was applied to capture the images and quantified by using the Fusion CAPT software (Vilber Lourmat, France).

2.6 Detection of RhoA Activity by G-LISA Assay

Ciliary body tissues of guinea pigs from each group were isolated and placed on ice, followed by protein extraction using ice-cold lysis buffer and subsequent protein quantification. RhoA activity was determined by the G-LISA® RhoA Activation Assay (BK124-L, cytoskeleton, USA). Protein concentrations were normalized to 0.2 mg/mL, and samples were loaded in triplicate along with blank and positive controls onto RhoA-GTP coated plates. After incubating at 4 °C for 30 min with shaking, the plates were washed and incubated with anti-RhoA primary antibody (45 min, room temperature, 400 rpm), followed by a secondary antibody under the same conditions. HRP substrate was added after the final washes, and the reaction was stopped after 15 min at 37 °C. Absorbance was measured at 490 nm using a microplate reader.

2.7 RT^2 profiler™ PCR Array for Fibrosis

To explore the changes in fibrosis-related gene expression in the ciliary body of the LIM guinea pigs, the RT^2 Profiler™ PCR Array (Qiagen, Germany) for fibrosis was used. Briefly, RNA from the ciliary body in the NC and LIM groups was extracted after myopia induction for 2 weeks, and cDNA was synthesized (AG0302-B, Sparkjade, China). The PCR array assay was performed according to the manufacturer's instructions. The cycle threshold (CT) values were calculated using the PCR machine's program, followed by PCR array data analysis.

2.8 Ingenuity Pathway Analysis (IPA)

Differentially expressed genes (DEGs) were defined as those meeting the following criteria: a false discovery rate (FDR) of <0.01, an absolute fold change of ≥ 1.5, and a p-value < 0.05. IPA is a web-based software application (http://www.ingenuity.com) that identifies biological pathways and functions associated with biomolecules. After uploading the screened DEGs to the IPA bioinformatics analysis suite (version 1.0, QIAGEN, DUS, Germany), IPA classical signaling pathway analysis, disease and functional analysis, upstream regulatory factor analysis, and downstream disease and functional enrichment analysis were performed.

2.9 PacBio Sequencing

After 2 weeks of myopia induction, the ocular ciliary body of guinea pigs in the NC and LIM groups was separated under sterile conditions, and total RNA was extracted and purified. The RNA integrity number (RIN) was assessed after purification, and the total RNA content was ≥ 2 µg, the RIN value was ≥ 8, and the OD value/280 ratio was 2.0~2.2 for each sample (n = 3). A single-molecule real-time (SMRT) sequencing platform was used to perform PacBio sequencing for each sample. DESeq2 was used to identify differentially expressed (DE) genes in the NC and LIM groups, employing screening criteria of a fold change between groups $\geq \pm 1.5$ and an adjusted p value $<$ 0.05. Gene annotation enrichment analysis was then performed on the differentially expressed genes using Metascape (https://metascape.org).

2.10 Masson's Staining

After 6 weeks of myopia induction, the eyes from the NC, LIM, and Y27632 groups were separated and immediately placed in EP tubes containing fixative solution for 24 h for routine dehydration, paraffin embedding, and sectioning for Masson's staining (Servicebio Co., Ltd., Wuhan, China) (n = 3). Briefly, eyeballs were fixed with 4% paraformaldehyde, and the sections were subjected to routine dehydration, paraffin embedding, and dewaxing in water. After overnight incubation with potassium dichromate, ferric hematoxylin, phosphomolybdate, aniline blue, and ponceau acid magenta were used for staining. Finally, the sections were dehydrated and then sealed. With this staining method, collagen fibers appear blue, muscle fibers appear red, and cell nuclei appear blue-black.

2.11 Immunohistochemistry (IHC)

After fixing the ciliary body tissue with eye fixative, it was subjected to routine dehydration, paraffin embedding, sectioning, and dewaxing. The tissue sections were then blocked with 5% bovine serum albumin, followed by incubation with α-SMA and Col-1 primary antibodies at 4 °C overnight. After washing with PBS, the tissue sections were incubated with a secondary antibody at 37 °C for 30 min. Subsequently, the samples were washed with PBS and subjected to DAB staining. Finally, tissue sections were imaged under a light microscope, and the resulting micrographs were quantified using ImageJ software.

2.12 Immunofluorescence (IF)

After 6 weeks of myopia induction, the eyeballs were separated (n = 3). The same procedure was performed as described for IHC. After antigen retrieval, the sections were washed with PBS (5 min × 3) and blocked with BSA, which was added dropwise, for 30 min. The primary antibody against TGF-β1 was added dropwise, followed by incubation at 4 °C overnight. The tissue sections were then incubated with a secondary antibody for 50 min, followed by incubation in the dark with DAPI staining solution for 10 min. The tissue sections were quenched with an autofluorescence quencher for 5 min, sealed with an antifluorescence quencher, and observed by a fluorescence microscope (Nikon, Eclipse, 55i, Tokyo, Japan).

2.13 Transmission Electron Microscopy (TEM)

The right eyes of the guinea pigs in the NC and LIM groups (n = 3) were immersed in electron microscope fixation solution (Wuhan Sevier Biotechnology Co., Ltd., Wuhan, China) at 4 °C for 4 h. Next, the ciliary body tissue was cut to approximately 1 mm × 1 mm × 1 mm, fixed for 24 h, washed with PBS, and then fixed with 1% osmium acid. The sections were subsequently rinsed with gradient ethanol and dehydrated with acetone. Finally, the tissue sections were observed via TEM (Hitachi, Ltd., HT7700, Japan).

2.14 Young's Modulus

Young's modulus is a physical quantity that describes the resistance of a solid material to deformation. It is also referred to the tensile modulus. Young's modulus is the most common type of elastic modulus, and it measures the stiffness of an isotropic elastomer. The mechanical properties of guinea pig ciliary body tissue from each group were evaluated using the Piuma nanoindentation system (OPTICS11, Amsterdam, Netherlands) (n = 3). To minimize the effects of post-mortem tissue autolysis and alterations in biomechanical properties, all nanoindentation tests were completed within 60 min post-enucleation. The entire testing procedure was conducted at a physiological temperature of 37 °C to simulate the *in vivo* environment, utilizing a stage-top incubator system. To prevent dehydration and subsequent stiffening of the tissue, the ciliary body samples were continuously immersed in pre-warmed PBS throughout the indentation process, ensuring normal hydration and mechanical properties. All indentation tests were performed using a spherical tip with a radius of 27 µm and a cantilever with a stiffness of 0.49 N/m, and the indentation was applied at the center of each piece of ciliary tissue. The elastic modulus of the ciliary tissue was determined, and the data were analyzed using DataViewer v2 (Amsterdam, the Netherlands).

2.15 Noninvasive Micro-Test Technology (NMT)

NMT (Younger USA LLC) was used to measure Ca^{2+} fluxes in the ciliary body tissues of guinea pigs in each group, using a 35 mm cell culture dish. Firstly, prepare, install, and calibrate Ca^{2+} selective microelectrodes. Fill the back of the glass microsensor with electrolyte (100 mmol/L $CaCl_2$), with a length of about 1 cm from the tip; then fill the tip of the glass microsensor with 40 µm of Ca^{2+} liquid ion exchanger (XY-SJ Ca, Younger US); After calibration with 1 mmol/L, 0.5 mmol/L, and 0.05 mmol Ca^{2+} calibration solutions, electrodes with slopes >22 mV/decade can be used for subsequent detection. After 6 weeks of myopia induction, the ciliary body tissue of each group of guinea pigs was isolated under sterile conditions (n = 3), immobilized in PBS, and then placed in the test solution. To measure the changes in Ca^{2+} concentration occurring outside the tissue membrane, the electrode movement frequency, or sampling frequency, was set at 0.3 Hz. After recording for 5 min, the raw data microvolt differences ($\Delta\mu V$) were imported and converted into the Ca^{2+} flux using JCal version 3.3 (Miami, FL, USA).

2.16 Functional Experiments on the Intervention Effect of ROCK Inhibitors

To clarify the primary driving role of TGF-β/RhoA/ROCK pathway activation in myopic ciliary body EMT and fibrosis, we performed functional validation experiments using the ROCK inhibitor Y-27632. After 6 weeks of Y-27632 intervention, the binocular refraction and axial length of myopic guinea pigs were measured. Additionally, Masson staining, IHC, and IF assays were combined to further explore the levels of ciliary body EMT and fibrosis following Y-27632 intervention.

2.17 Statistical Analysis

The results are presented as means ± SEM, and SPSS statistical software (SPSS Version 20.0, Chicago, USA) was used to analyze the data. For comparisons across multiple groups, we first assessed normality and homogeneity of variance. Upon confirmation, one-way ANOVA was applied, followed by Tukey's post hoc test for all pairwise comparisons. $p < 0.05$ was considered significantly different. Unless otherwise noted, each experiment was repeated three or more times with biologically independent samples.

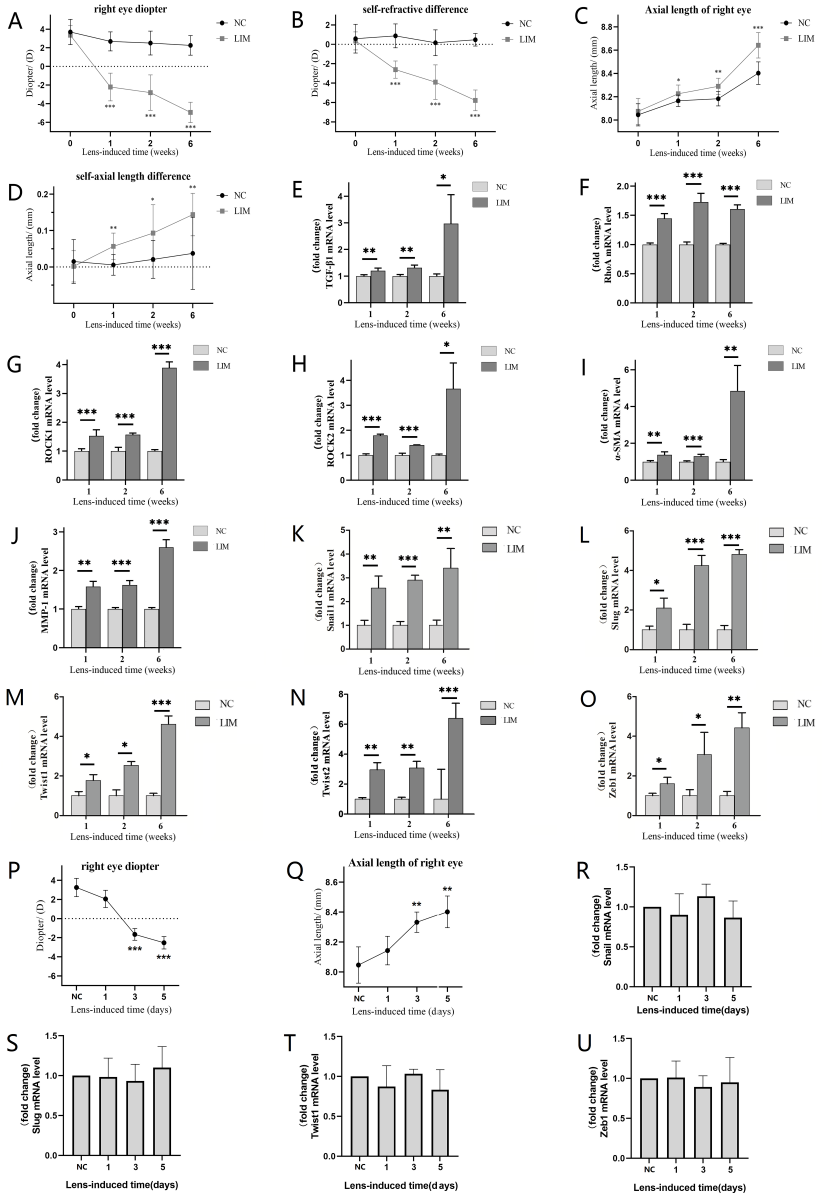

Fig. 1. Changes in diopter, axial length, TGF-β/RhoA/ROCK signaling pathway, EMT transcription factors, and fibrosis-related genes in the ciliary body of guinea pigs in each group after 1-, 2-, and 6-week myopia induction. (A) The diopter of the right eye in the LIM group was significantly higher than that in the NC group. (B) The diopter difference between the right eye and the left eye in the LIM group was significantly increased compared with the NC group. (C) The axial length of the right eye in the LIM group increased compared with the NC group. (D) The difference between the axial lengths of the right eye and the left eye in the LIM group was significant. (E) The expression of *TGF-β1* mRNA. (F) The expression of *RhoA* mRNA. (G) The expression of *ROCK1* mRNA. (H) The expression of *ROCK2* mRNA. (I) The expression of α-*SMA* mRNA. (J) The expression of *MMP1* mRNA. (K) The expression of *Snail1* mRNA. (L) The expression of *Slug* mRNA. (M) The expression of *Twist1* mRNA. (N) The expression of *Twist2* mRNA. (O) The expression of *Zeb1* mRNA. (P) The diopter changes of the right eye in the LIM group in the ultra-early stage of lens-induced myopia. (Q) The axial length changes of the right eye in the LIM group in the ultra-early stage of lens-induced myopia. (R) The expression of *Snail1* mRNA in the ultra-early stage of lens-induced myopia. (S) The expression of Slug mRNA in the ultra-early stage of lens-induced myopia. (T) The expression of *Twist1* mRNA in the ultra-early stage of lens-induced myopia. (U) The expression of *Zeb1* mRNA in the ultra-early stage of lens-induced myopia. All RT-qPCR data are presented as mean $\pm$ standard error of the mean (SEM) (n = 6). *$p <$ 0.05, **$p < 0.01$, and ***$p < 0.001$. *TGF*, transforming growth factor; *RhoA*, Ras homolog family member A; *ROCK*, Rho-associated protein kinase; α-*SMA*, α-smooth muscle actin; *MMP*, matrix metalloproteinase; LIM, lens-induced myopia; NC, normal control.

3. Results

3.1 Changes in Diopter Values and Axial Lengths

Before myopia induction, there were no statistically significant differences in diopter values (NC vs. LIM. 3.70 ± 1.36 D vs. 3.35 ± 1.03 D) or axial lengths (NC vs. LIM. 8.04 ± 0.09 mm vs. 8.07 ± 0.11 mm) between the NC and LIM groups ($p > 0.05$). After 1, 2, and 6 weeks of myopia induction, the diopter values (NC vs. LIM. 1 w: 2.68 ± 1.02 D vs. –2.20 ± 1.49 D; 2 w: 2.52 ± 1.28 D vs. –2.81 ± 1.91 D; 6 w: 2.27 ± 1.05 D vs. –4.93 ± 1.10 D) of the right eyes in the LIM group were significantly greater than those in the NC group (all $p < 0.001$) (Fig. 1A). Compared with those in the NC group, the differences in diopter values (NC vs. LIM. 1 w: 0.87 ± 1.22 D vs. –2.60 ± 0.88 D; 2 w: 0.16 ± 1.32 D vs. –3.89 ± 1.77 D; 6 w: 0.47 ± 0.65 D vs. –5.77 ± 1.07 D) between the right eyes and the left eyes in the LIM group were significantly greater (all $p < 0.001$) (Fig. 1B). After 1 week, 2 weeks and 6 weeks of lens-induced myopia, the axial lengths (NC vs. LIM. 1 w: 8.17 ± 0.05 mm vs. 8.23 ± 0.08 mm; 2 w: 8.18 ± 0.06 mm vs. 8.29 ± 0.07 mm; 6 w: 8.40 ± 0.10 mm vs. 8.72 ± 0.13 mm) of the right eyes in the LIM group were significantly greater than those in the NC group (all $p < 0.05$) (Fig. 1C), and the differences in axial length (NC vs. LIM. 1 w: 0.00 ± 0.02 mm vs. 0.05 ± 0.03 mm; 2 w: 0.02 ± 0.05 mm vs. 0.09 ± 0.07 mm; 6 w: 0.03 ± 0.09 mm vs. 0.14 ± 0.05 mm) between the right eyes and the left eyes were significantly greater than those in the NC group (all $p < 0.05$) (Fig. 1D). Moreover, during the process of lens-induced myopia, the body weight, food intake and other behavioral activities of guinea pigs in the LIM group did not significantly chang from those in the NC group.

3.2 TGF-β/RhoA/ROCK Signaling Pathway, EMT Transcription Factors, and Fibrosis-Related Genes in Ciliary Body

After 1, 2, and 6 weeks of myopia induction, the mRNA expression levels of *TGF-β1* (Fig. 1E), *RhoA* (Fig. 1F), *ROCK1* (Fig. 1G), *ROCK2* (Fig. 1H), *α-SMA* (Fig. 1I), and *MMP1* (Fig. 1J) in the ciliary body of the LIM group were significantly greater than those in the NC group (all $p < 0.01$), and these TGF-β/RhoA/ROCK signaling pathway components and fibrosis-related genes increased more significantly after 6 weeks of myopia induction. Furthermore, the mRNA expression levels of EMT transcription factors such as *Snail1* (Fig. 1K), *Slug* (Fig. 1L), *Twist1* (Fig. 1M), *Twist2* (Fig. 1N), and *Zeb1* (Fig. 1O) in the ciliary body of the LIM group were significantly higher than those in the NC group after 1-, and 2-week myopia induction (all $p < 0.01$), confirming that EMT occurred in the ciliary body at the early stage of myopia. However, to clarify whether EMT-mediated fibrosis is the initiating event or merely a consequence of prior functional alterations, we dynamically monitored EMT transcription factors, refractive error, and axial length parameters at ultra-early time points (1, 3, and 5 days). This aimed to evaluate the relationship between the temporal sequence of EMT and functional changes with earlier times. Results showed that on day 1 after lens induction, there were no significant differences in the refractive error or axial length of the right eye between the LIM group and the NC group (Fig. 1P,Q), nor were there notable changes in the mRNA levels of EMT-related transcription factors (Fig. 1R–U). On days 3 and 5 after lens induction, the refractive error and axial length of the right eye in the LIM group increased significantly (all $p < 0.01$), while the mRNA levels of EMT-related transcription factors remained unchanged (Fig. 1R–U). These findings indicate that functional changes, such as increases in biological parameters of refractive error and axial length, occur earlier than alterations in EMT transcription factor levels during the ultra-early stage of lens-induced myopia. This suggests that EMT-mediated fibrosis is not an initiating event but merely a consequence of prior functional modifications.

3.3 TGF-β/RhoA/ROCK Signaling- and Fibrosis-Related Proteins in the Ciliary Body

As shown in Fig. 2A, after 1, 2, and 6 weeks of myopia induction, the protein levels of TGF-β1 (Fig. 2B), ROCK1 (Fig. 2D), and ROCK2 (Fig. 2E) in the ciliary body of LIM eyes were significantly greater than in the NC group (all $p < 0.05$). In addition, the protein expression of RhoA (Fig. 2C), α-SMA (Fig. 2F), and MMP1 (Fig. 2G) in the ciliary body of LIM eyes was significantly greater in the LIM group than in the NC group (all $p < 0.01$), and the increases were especially significant at 6 weeks after myopia induction (all $p < 0.01$). The protein expression of N-cadherin (Fig. 2H,J) in the ciliary body of guinea pig eyes in the LIM group after inducing myopia for 1, 2, and 6 weeks was significantly higher than that in the NC group (all $p < 0.05$). After inducing myopia for 2 and 6 weeks, the expression of E-cadherin (Fig. 2H,I) protein in the ciliary body of guinea pig eyes in the LIM group increased (all $p < 0.05$), and the expression was particularly significant at 6 weeks after inducing myopia (all $p < 0.05$). Moreover, the results showed that after inducing myopia for 1, 2, and 6 weeks, the activity of RhoA in the ciliary body of guinea pigs in the LIM group was higher than that in the NC group (Fig. 2K) (all $p < 0.05$), and it was particularly significant at 6 weeks, suggesting that the occurrence and development of myopia are closely related to the activation of the RhoA signaling pathway.

3.4 Fibrosis RT^2 Profiler PCR Array

Fig. 3 shows that there were 42 DEGs in the LIM group (vs. NC), including 35 upregulated DEGs (red) and 7 downregulated DEGs (blue) (Fig. 3A). Further analysis of the DEGs revealed that the upregulated genes accounted for 41.67% of the 84 gene arrays, and 31.43% of the upregulated genes had differential multiples ≥2.0, indicating that

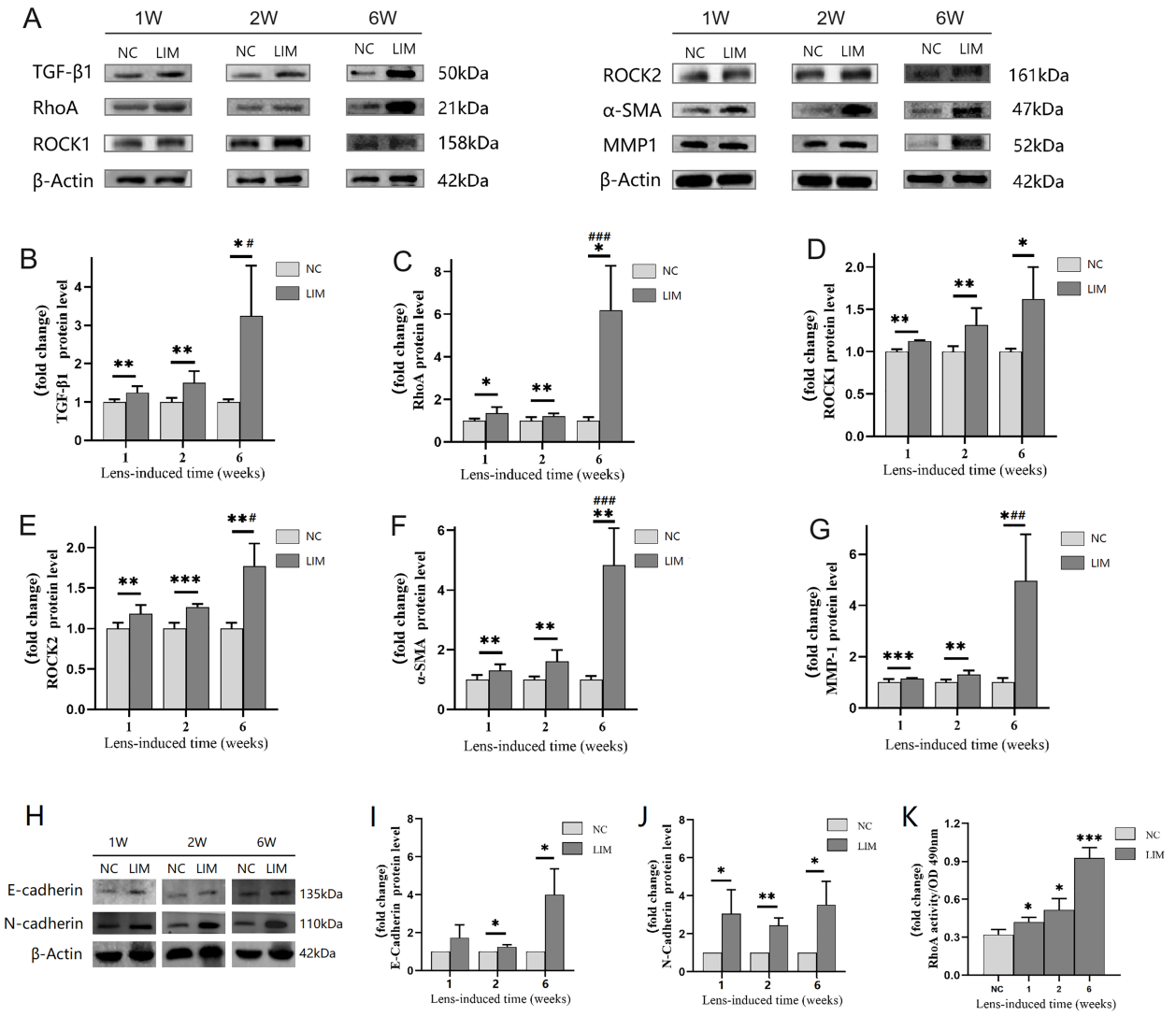

Fig. 2. The protein levels related to the TGF-β/RhoA/ROCK signaling pathway and fibrosis in the ciliary body. (A) TGF-β/RhoA/ROCK signaling pathway and fibrosis related protein expression. (B–G) Histogram of optical density analysis in TGF-β1, RhoA, ROCK1, ROCK2, α-SMA and MMP-1 proteins. (H) Expression of E-cadherin and N-cadherin proteins. (I) Histogram of optical density analysis in E-cadherin protein. (J) Histogram of optical density analysis in N-cadherin protein. (K) G-LISA detection of RhoA activity. All data are presented as mean ± SEM (n = 6). Compared with the NC group, $^{*}p < 0.05$, $^{**}p < 0.01$, and $^{***}p < 0.001$. Compared with the LIM group in week 1, $^{\#}p < 0.05$, $^{\#\#}p < 0.01$, and $^{\#\#\#}p < 0.001$.

many fibrosis-related mechanisms were activated in the ciliary body of guinea pigs with myopia (Fig. 3B). Moreover, cluster analysis of the expression degree of DEGs in all the groups revealed upregulated genes related to fibrosis, which involved mainly Tgfbr2, Col3a1, Col1a2, and Hgf, as well as matrix metalloproteinase (MMP) family genes (Mmp2, Mmp3, Mmp9, and Mmp14). These findings suggested that the pathological process of myopia is associated with the activation of the TGF-β signaling pathway and the involvement of tissue repair processes such as fibrosis (Fig. 3C).

3.5 IPA

IPA revealed that the pathways associated with the DEGs were activated in the LIM group compared with those in the NC group (Fig. 3D), and these pathways involved mainly the osteoarthritis pathway, the hepatic fibrosis signaling pathway, the regulation of EMT by the growth factor pathway, and the TGF-β signaling pathway. Disease and function analyses of the DEGs revealed that the differential genes in the LIM group (vs. the NC group) were related mainly to cellular growth and proliferation, cellular movement, cellular development, and immune cell trafficking. In addition, the DEGs in the LIM group (vs. the NC group) affected organizational development, organizational injury and abnormalities, connective tissue development, and function (Fig. 3E). Thus, during the development of myopia, cell metabolism and homeostasis may be significantly affected, and the development and function of tissues

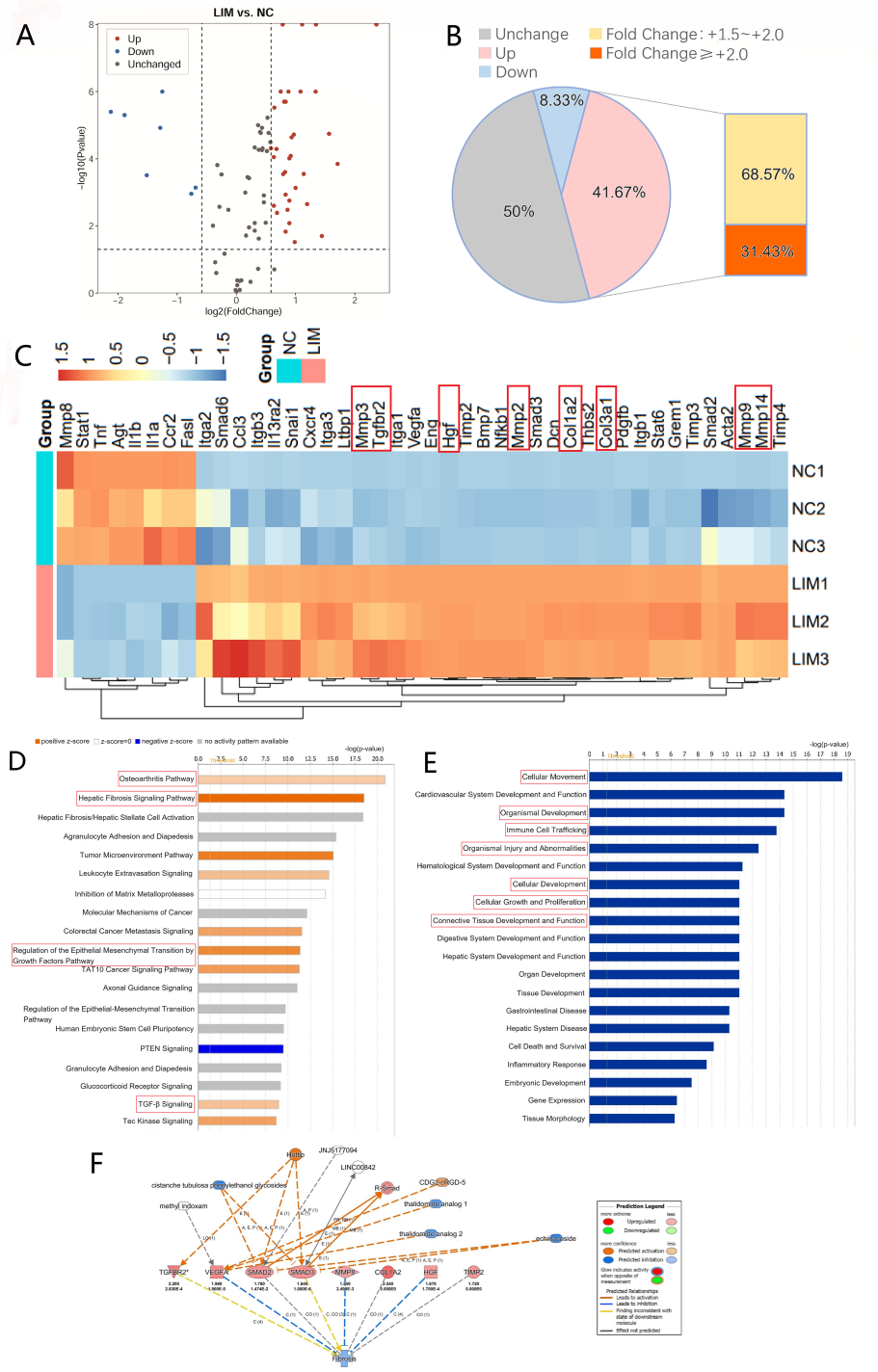

Fig. 3. Changes in 84 gene levels related to fibrosis and Ingenuity pathway analysis of DEGs in the ciliary body fibrosis PCR array of the LIM group in the ciliary body tissue of each group after 2-week myopia induction (n = 3). (A) Volcano map of 84 fibrosis related genes, compared with the NC group, among the DEGs in the LIM group with a fold difference $\geq \pm 1.5$ and $p < 0.05$. (B) Pie chart of 84 fibrosis-related genes in different categories. (C) Heat maps of 42 DEGs detected by 84 gene array of fibrosis, the gene clustering was enrichment analyzed based on the similarity of gene expression between samples. (D) IPA classical signaling pathway analysis. (E) Disease and functional analysis. (F) Upstream regulatory factors and downstream disease and function enrichment analysis. DEGs, Differentially expressed genes; IPA, Ingenuity pathway analysis.

and organs in the body may be significantly altered, eventually leading to tissue damage and abnormalities (Fig. 3E). Moreover, the upregulation of MMP8 and HGF may lead to the inhibition of ciliary body fibrosis in guinea pigs with myopia (Fig. 3F).

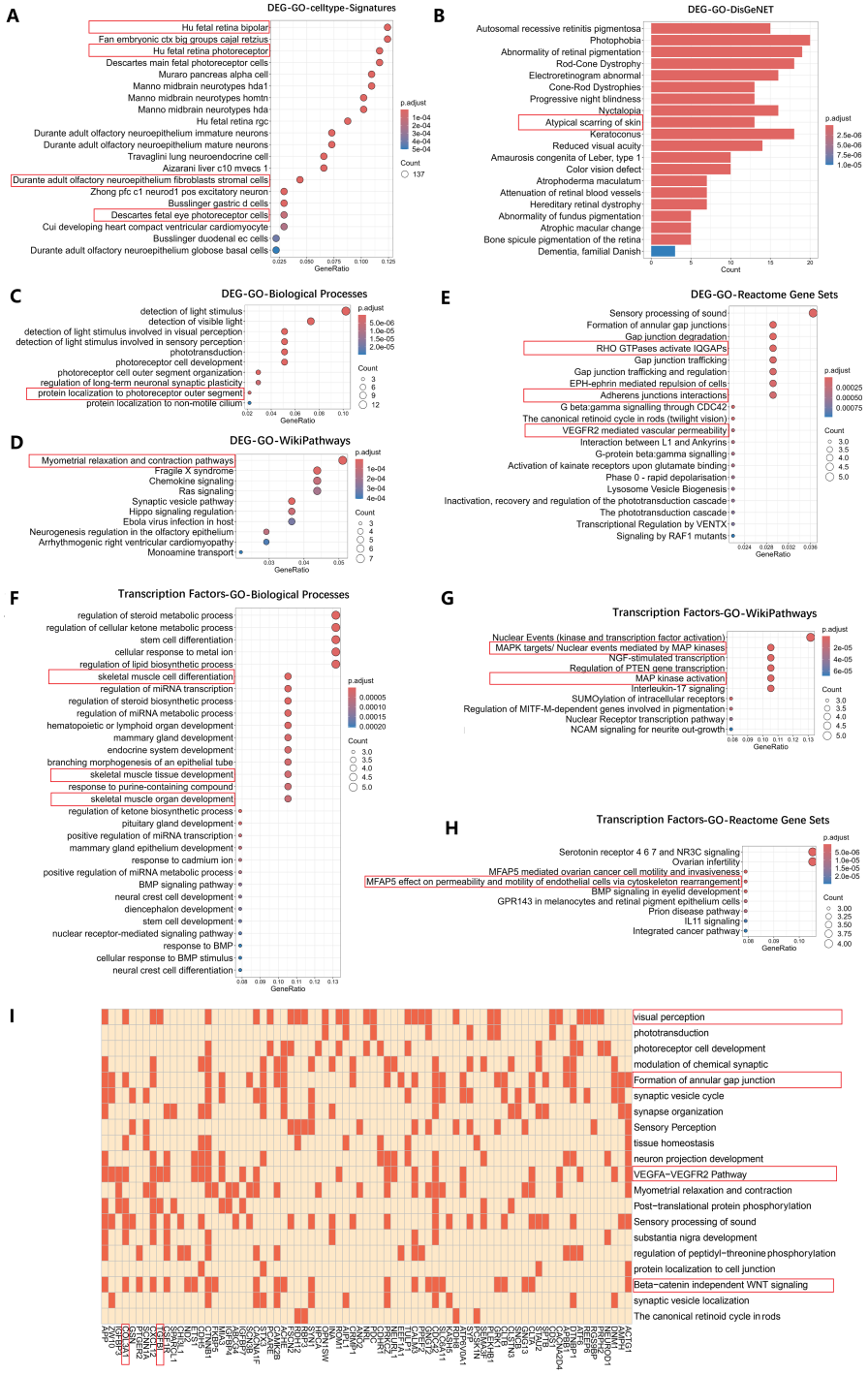

Fig. 4. GO enrichment analysis of the differentially expressed mRNAs and Transcription factor targets. (A) Celltype dotplot of differentially expressed genes (DEGs). (B) DisGeNet barplot of DEGs. (C) Biological process (BP) dotplot of DEGs. (D) WikiPathways dotplot of DEGs. (E) Reactome Gene set dotplot of DEGs. (F) Biological process (BP) dotplot of Transcription factor targets. (G) WikiPathways dotplot of Transcription factor targets. (H) Reactome gene set dotplot of Transcription factor. (I) DEGs distribution map.

3.6 PacBio Sequencing

In total, 139 DEGs were identified in the ciliary muscle tissue of guinea pigs in the NC group and LIM group, including 29 upregulated genes and 120 downregulated genes. The cell type dot plot revealed that the DEGs were associated mainly with fetal retina bipolar cells, fetal retina photoreceptor cells, adult olfactory neuroepithelial stromal fibroblasts and fetal eye photoreceptor cells (Fig. 4A), and atypical scarring of the skin was enriched in the analysis of the disease gene network (Fig. 4B). GO enrichment analysis revealed that these DEGs were related mainly to the

biological process of protein localization to the photoreceptor outer segment (Fig. 4C) and to the myometrial relaxation and contraction pathways (Fig. 4D), which provides evidence for the observed dysfunction of ciliary body elasticity in myopia. In addition, RHO GTPase activation of IQGAPs, adherens junction interactions, and VEGFR2-mediated vascular permeability were enriched in the Reactome gene sets (Fig. 4E). IQGAPs are key effector proteins and intersections of RhoA and Rac1. Enrichment analysis suggests significant changes in the activity of the Rho GTPase family (including RhoA) in the myopic ciliary body. GO enrichment analysis of the transcription factor targets of the DEGs revealed associations with the following terms: skeletal muscle cell differentiation, skeletal muscle tissue development, and skeletal muscle organ development (Fig. 4F); MAPK targets/nuclear events mediated by MAP kinases and MAP kinase activation (Fig. 4G); and the effect of MFAP5 on the permeability and motility of endothelial cells via cytoskeleton rearrangement (Fig. 4H). Notably, the COL3A1 and TGFβ1 DEGs were involved in visual perception, the formation of annular gap junctions, the Beta-catenin-independent WNT signaling pathway, and other biological functions according to the DEG distribution map (Fig. 4I), suggesting the activation of the TGF-β/RhoA signaling pathway and the occurrence of fibrosis in myopic body tissues. These findings indicated that myometrial relaxation and contraction pathways, as well as adhesion junction interactions, are involved in the occurrence of myopia, which is strongly correlated with ciliary body fibrosis.

3.7 Masson's Staining and IHC

Compared with that in the NC group, the degree of fibrosis (as indicated by blue color) (NC vs. LIM. $0.24763159 \pm 0.013337\%$ vs. $0.408256574 \pm 0.013965\%$) in the ciliary body of guinea pigs in the LIM group was aggravated after 6 weeks of myopia induction (Fig. 5A,B). In addition, immunohistochemistry was utilized to evaluate the levels of α-SMA and Col-1 in the ciliary body tissues of guinea pigs with myopia. The expression of α-SMA (NC vs. LIM. $0.1734483 \pm 0.0431506\%$ vs. $0.3568124 \pm 0.0344084\%$) and Col-1 (NC vs. LIM. $0.24763159 \pm 0.013337\%$ vs. $0.408256574 \pm 0.013965\%$) in the ciliary body of guinea pigs in the 6-week LIM group was greater than that in the NC group (Fig. 5C,D), suggesting that ciliary body fibrosis and activation of fibroblasts occurred in the process of myopia.

3.8 IF

In Fig. 5, the nuclei stained with DAPI appear blue, and the corresponding fluorescein-labeled positive expression of α-SMA (Fig. 5E) and Col-1 (Fig. 5F) is shown in red. The expression of α-SMA (NC vs. LIM. $0.1691442 \pm 0.0258369\%$ vs. $0.616374 \pm 0.0341538\%$) and Col-1 (NC vs. LIM. $0.1174157 \pm 0.0608709\%$ vs. $0.7198452 \pm 0.0560648\%$) in the ciliary body tissue of the LIM group was greater than that in the NC group (Fig. 5G), indicating the myofibroblast activation and ciliary body fibrosis in the pathological process of myopia.

3.9 TEM

The structural characteristics of the ciliary body in each group were evaluated by TEM. The epithelial cells in the NC group had a complete cell membrane, a regular morphology, tight cell connections, and fewer fibroblasts (Fig. 6A). In the LIM group, the epithelial cells lacked a regular morphology, and the cells were slender, with fibroblast-like characteristics, indicating the occurrence of ciliary body EMT and fibrosis in myopia (Fig. 6B).

3.10 Young's Modulus

Young's modulus is the ratio of stress (σ) to strain (ϵ) in the linear elastic deformation stage of a structured material. Young's modulus is the core quantitative index of the elastic properties of a structured material, and it directly reflects the resistance of a structured material to external forces in the elastic deformation stage. After 6 weeks of myopia induction, the Young's modulus of the ciliary body tissue in the guinea pigs in the NC and LIM groups was measured. Compared with the NC group, the LIM group presented an increase in the Young's modulus of the ciliary body tissue in guinea pigs (Fig. 6C–G). A higher Young's modulus indicates a stiffer structure and therefore a smaller elastic deformation for a given applied load. The increase in elastic modulus and decrease in elasticity of the ciliary body tissue in the LIM group guinea pigs further confirmed the occurrence of fibrosis in the ciliary body of guinea pigs with myopia.

3.11 NMT

After 6 weeks of myopia induction, the Ca^{2+} levels in the ciliary body tissue of guinea pigs in the NC and LIM groups were measured via NMT (Fig. 6H). Abnormal intracellular Ca^{2+} regulation is involved in the occurrence and development of tissue fibrosis, and an increase in the intracellular Ca^{2+} level can promote tissue fibrosis. Compared with that in the NC group, the level of Ca^{2+} inflow in the ciliary body tissue of guinea pigs in the LIM group was increased, which indicated that the occurrence of myopia was related to the aggravation of ciliary body fibrosis (Fig. 6I,J).

3.12 ROCK Inhibition Attenuates Myopia and Ciliary Body Fibrosis

The results showed that after Y-27632 intervention, both the refractive error of the right eye and the interocular refractive error difference in guinea pigs were lower than those in the lens-induced myopia (LIM) group (Fig. 7A,B) (all $p < 0.05$), and the axial length as well as the interocular axial length difference were also significantly improved (Fig. 7C,D) ($p < 0.05$). Masson staining revealed that com-

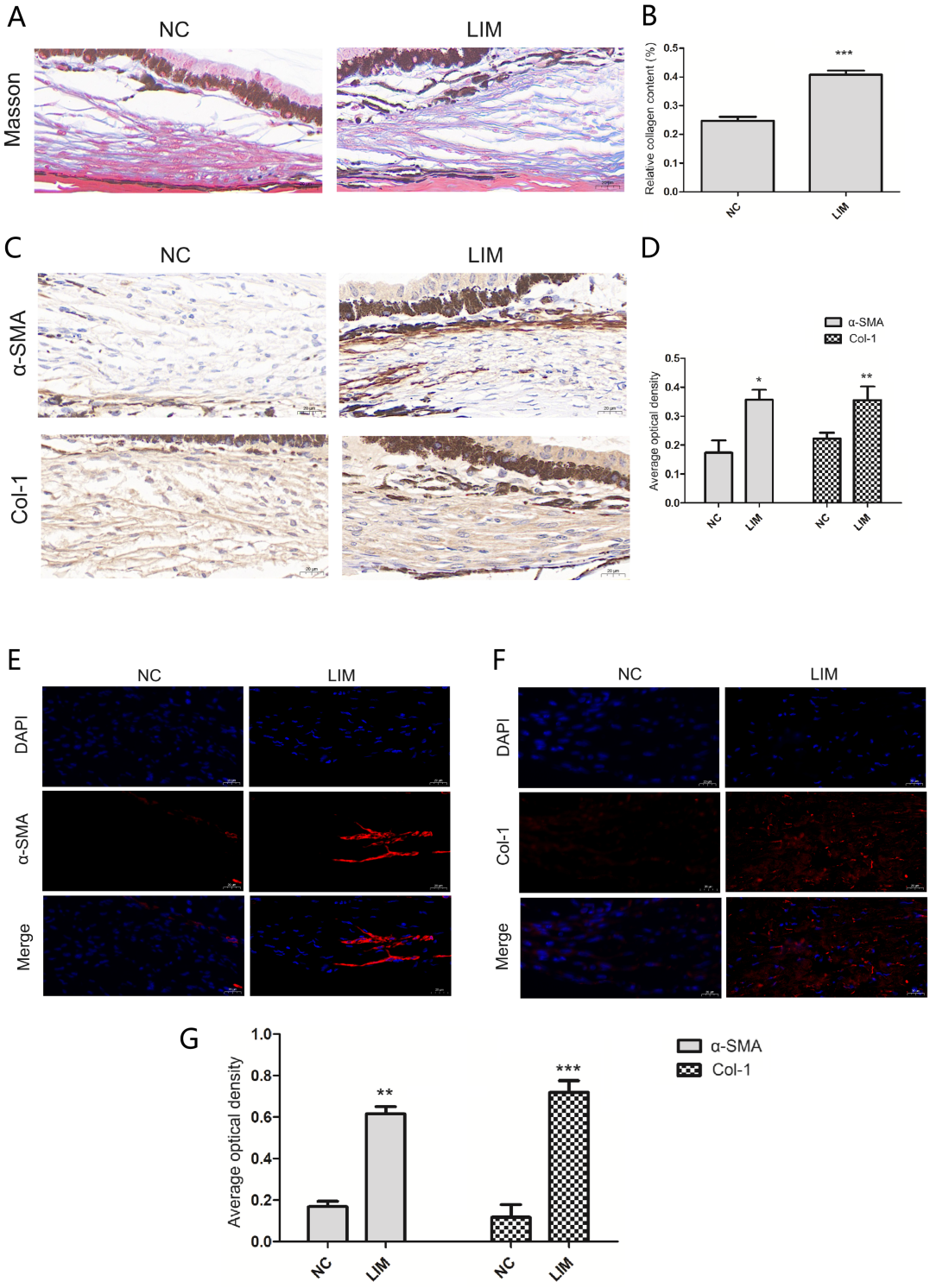

Fig. 5. The fibrotic progression of the ciliary body tissue detected by Masson Staining, immunohistochemistry, and immunofluorescence after 6-week myopia induction. (A) Masson Staining (400×), Bar = 20 µm. (B) Histogram of relative collagen content analysis. Compared with the NC group, ***$p < 0.001$. (C) Immunohistochemistry (400×), Bar = 20 µm. (D) Histogram of optical density analysis in α-SMA and Col-1 proteins. Compared with the NC group, *$p < 0.05$ and **$p < 0.01$. (E) The α-SMA levels in the ciliary body (400×), Bar = 20 µm. (F) The Col-1 levels in the ciliary body (400×), Bar = 20 µm. (G) Histogram of optical density analysis in α-SMA and Col-1 proteins. All data are presented as mean ± SEM (n = 3). Compared with the NC group, **$p < 0.01$, and ***$p < 0.001$.

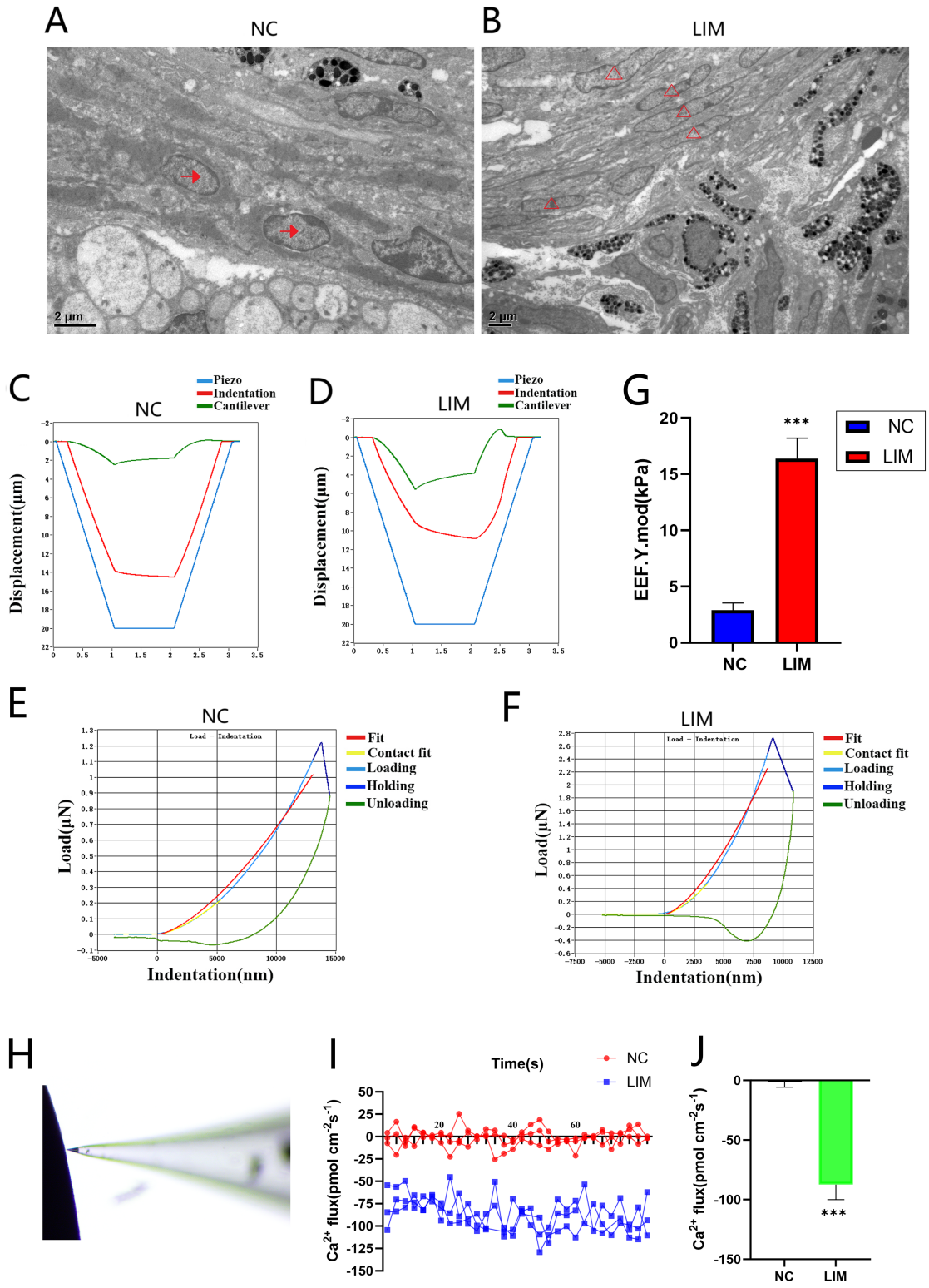

Fig. 6. The ciliary body of the NC group and LIM group was observed by TEM, Piuma nanoindentation system, and Non-invasive Micro-Test Technology (NMT) after 6-week myopia induction (10000×). All data are presented as mean ± SEM (n = 9). (A) The ciliary body of the NC group was observed by TEM. Bar = 2 μm. (B) The ciliary body of the LIM group was observed by TEM (n = 3). → : Epithelial Cells, △: Fibroblasts. Bar = 2 μm. (C,D) Displacement-time curve. (E,F) The load-indentation curve of the nanoindentation test depicts the dynamic change of load and indentation from load to hold to unloading when subjected to external force. (G) Young's modulus statistic plot (n = 3). Compared with the NC group, ***$p < 0.001$. (H) NMT operation chart, (I) Ca^{2+} flux, and (J) Analysis of Ca^{2+} flux (n = 3). Compared with the NC group, ***$p < 0.001$. TEM, Transmission electron microscopy.

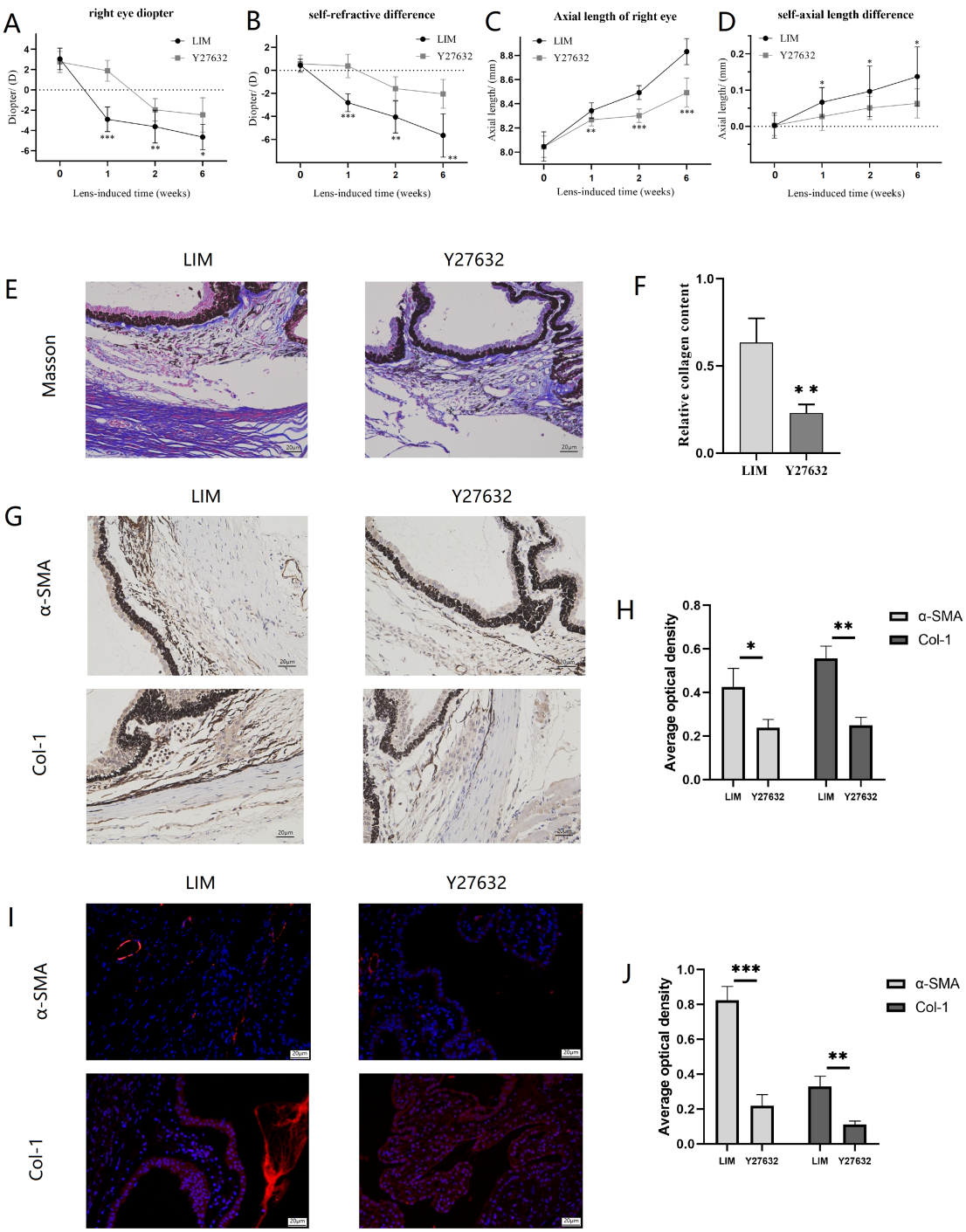

Fig. 7. The ocular biological parameters, ciliary body EMT and fibrosis levels of myopic guinea pigs after inhibiting ROCK for 6 weeks. (A) Refractive error of the right eye in guinea pigs from the LIM group and Y-27632 group. (B) Interocular difference in refractive error between the right and left eyes of individual guinea pigs in the LIM group and Y-27632 group. (C) Axial length of the right eye in guinea pigs from the LIM group and Y-27632 group. (D) Interocular difference in axial length between the right and left eyes of individual guinea pigs in the LIM group and Y-27632 group. (E) Masson Staining (400×), Bar = 20 μm. (F) Histogram of relative collagen content analysis. (G) Immunohistochemistry (400×), Bar = 20 μm. (H) Histogram of optical density analysis in α-SMA and Col-1 proteins. (I) The Col-1 levels in the ciliary body (400×), Bar = 20 μm. (J) Histogram of optical density analysis in α-SMA and Col-1 proteins. All data are presented as mean ± SEM (n = 3). Compared with the LIM group, *$p < 0.05$, **$p < 0.01$, and ***$p < 0.001$.

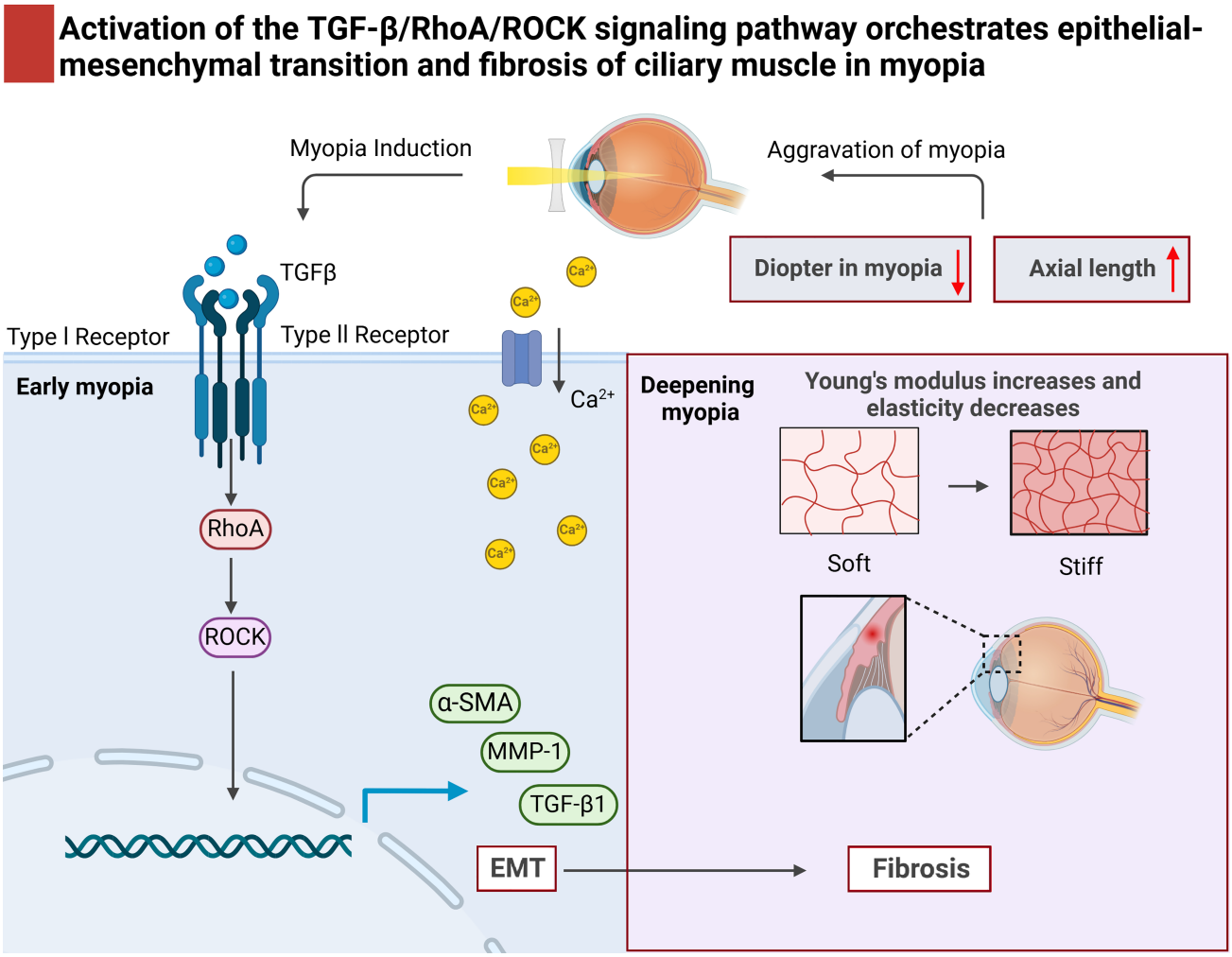

Fig. 8. Activation of the TGF-β/RhoA/ROCK signaling pathway orchestrates epithelial-mesenchymal transition and fibrosis of the ciliary body in myopia. (1) In the early stage of myopia, the activation of TGF-β/RhoA/ROCK signaling pathway and EMT in the ciliary body; (2) In deepening myopia, the experimental myopic ciliary body Ca^{2+} inflow and elastic modulus increase, elasticity decreases, fibroblasts are activated, fibrosis worsens, accompanied by abnormal ciliary body tissue morphology in the aggravation of myopia; (3) The activation of the TGF-β/RhoA/ROCK signaling pathway induced epithelial mesenchymal transition in myopic ciliary body, leading to ciliary body fibrosis and dysfunction, thereby increasing myopic refraction and axial length, exacerbating the pathological progression of myopia. ↑: Increase; ↓: Reduce.

pared with the LIM group, the degree of ciliary body fibrosis in guinea pigs was reduced after Y-27632 intervention (Fig. 7E,F). Moreover, IHC and IF were used to evaluate the levels of α-SMA and Col-1 in the ciliary body tissues of myopic guinea pigs after ROCK inhibition. The expressions of α-SMA and Col-1 in the ciliary body of the group were lower than those in the LIM group (Fig. 7G–J), suggesting that ROCK inhibition can ameliorate the pathological levels of EMT and fibrosis in the ciliary body of myopic guinea pigs.

4. Discussion

Myopia is a common disease in children and adolescents, and it is primarily due to excessive axial growth, resulting in blurred vision [22]. It is predicted that 4.758 billion individuals in the world will suffer from myopia by 2050, 19.7% of whom will suffer from high myopia [23]. The accommodation system of the eye consists of the ciliary process, ciliary muscle, choroid, suspensory ligament, lens capsule, and lens [24]. Adaptive regulation occurs when the ciliary muscle and ciliary process move forward and inward to release the tension of the suspensory ligament attached to the lens capsule [25]. Therefore, as one of the main structures of the intraocular regulatory system, the ciliary body may be involved in the occurrence and development of myopia. Chen *et al.* [26] measured the position of the ciliary body in the lens when the ciliary muscle relaxes or contracts in a mouse, and they reported that ciliary muscle relaxation increases the distance between the ciliary body and the lens; in contrast, ciliary contraction causes the

ciliary body to move toward the lens. In addition, ultrasound biomicroscopy (UBM) and optical coherence tomography (OCT) can be used to quantify and locate the ciliary body *in vivo*, and the ciliary body of patients with myopia becomes larger and shrinks with age [27]. In this study, after 1 week, 2 weeks, and 6 weeks of myopia induction, the differences in diopter values and axial lengths between LIM eyes and control eyes were significantly greater than those in the NC group. Over time, the diopter value and axial length gradually increased with increasing duration of myopia induction. Therefore, we speculate that during the occurrence and development of myopia, a decrease in intraocular refractive adjustment ability leads to continuous contraction of the ciliary body, and the growth of the ocular axis is promoted by hyperopia defocus, which induces the development of myopia.

TGF-β signaling can control the transcriptional dysregulation of target genes related to cell proliferation and structure as well as the production of ECM proteins, including fibronectin, laminin, etc. [28]. TGF-β initiates the transformation of fibroblasts into antiapoptotic myofibroblasts following various injury stimuli, such as inflammation, injury, hyperglycemia, hypoxia, and apoptosis in the local environment [29,30]. Myofibroblasts express α-SMA (a myofibroblast marker), secrete ECM components (including MMP-1), induce the apoptosis of alveolar epithelial cells, and promote the development of pulmonary fibrosis [31–33]. In addition, TGF-β-induced EMT can also lead to the development of ocular fibrosis, such as anterior subcapsular cataracts and posterior capsular opacities [34]. MMPs degrade the ECM and decompose ECM substrates, including Col, laminin, fibronectin, hyaluronan, and proteoglycans [35,36]. MMP-1 is a major protease in the MMP family that specifically degrades Col-I, -II, -III, -V, and -IX [37]. MMP-1 is expressed in various cells, such as stromal fibroblasts, endothelial cells, and epithelial cells [38]. Under normal physiological conditions, the expression of MMP-1 is low, but under pathological conditions, MMP-1 expression may be significantly increased [39]. Wang *et al*. [40] reported that increased MMP-1 activity increases the decomposition of the ECM, leading to fibrosis. In the present study, myopia progression under lens induction increased the expression of TGF-β1, α-SMA, and MMP-1, indicating that myopia progression is involved in the aggravation of EMT and fibrosis.

ROCK is regulated by Rho-GTPases and is involved in the control of multiple physiological functions, including cell contraction, migration, proliferation, and adhesion. The Rho signaling pathway can be activated during fibrosis and is involved in in the development of tissue fibrosis. Additionally, the RhoA/ROCK signaling pathway is involved in EMT. TGF-β1 can rapidly activate the RhoA/ROCK signaling pathway, which further affects α-SMA production and cytoskeleton-mediated myopia induction, and it induces the formation of stress fibers and the expression of mesenchymal characteristics, thereby participating in the EMT process [41]. Ji *et al*. [29] reported that in pulmonary fibrosis, TGF-β1 stimulation of lung fibroblasts increases the expression of RhoA, RhoC, and ROCK1, indicating that the RhoA/ROCK pathway is involved in the proliferation, differentiation, and excessive deposition of the extracellular matrix of lung fibroblasts. Additionally, Masszi *et al*. [42] revealed that RhoA is involved in both cytoskeleton remodeling and the activation of the α-SMA promoter in TGF-β1-induced EMT in renal epithelial cells.

The ciliary muscle contains the ciliary epithelium, stroma, and muscle [43]. During EMT, epithelial cells lose their polygonal morphology and adherent cell contacts, and they gain fibroblast-like features, including elongated morphology, increased expression of mesenchymal markers, and motility. The present study demonstrated that the ciliary body of guinea pigs in the LIM group lacked regular epithelial cells, as evidenced by slender and fibroblast-like cells, accompanied by vacuoles after cell loss, indicating that EMT occurred in the ciliary body of LIM guinea pigs, which transformed normal epithelial cells into fibroblasts, accompanied by apoptosis. In addition, this study revealed that the expression of TGF-β1, RhoA, ROCK1, ROCK2, α-SMA, and MMP-1 in the ciliary body of LIM guinea pigs after 1, 2, and 6 weeks of myopia induction was significantly greater than that in the ciliary body of the NC group. During the development of myopia, we speculate that the ciliary myoepithelial cells in LIM guinea pigs are damaged, leading to the activation of TGF-β1 expression. This process converts epithelial cells into fibroblasts through the RhoA/ROCK signal transduction pathway, resulting in the formation of myofibroblasts and facilitating the EMT. Myofibroblasts specifically express α-SMA, secrete ECM components, and further participate in the development of tissue fibrosis, thereby influencing the regulatory function of the ciliary body.

Fibroblasts are activated by the stimulation of the TGF-β factor. The activated fibroblasts express α-SMA and form myofibroblasts. Fibroblasts can respond dynamically to environmental signals, exhibiting significant plasticity, transforming into various functional cell types, and adopting different activation states [44]. Fibroblasts in an activated state are present in the physiological conditions of normal wound healing and various diseases, such as chronic wound healing, tissue fibrosis, and cancer [45]. In response to injury, activated fibroblasts acquire the ability to migrate, produce ECM proteins, and become proto-myofibroblasts. These proto-myofibroblasts represent the intermediate stage before they mature into contractile myofibroblasts. Fully mature myofibroblasts highly express α-SMA and are involved in pathological processes such as fibrosis [46]. Persistent myofibroblasts are also produced by the transformation of endothelial cells into mesenchymal cells. Continuous myofibroblasts produce ECM but also express high levels of collagen genes and partic-

ipate in profibrotic signaling [47]. In addition, the plasticity of fibroblasts is affected by factors of the tissue itself, such as mechanical stress and tissue stiffness. When fibroblasts are placed in a hard microenvironment, they are more likely to transform into transient myofibroblasts that produce ECM [48]. Furthermore, it is inferred that Physical interactions with macrophages also further affect the activation of fibroblasts. A recent study has revealed that integrin-mediated binding between macrophages and fibroblasts triggers calcium (Ca^{2+}) influx in fibroblasts, driving contraction events leading to collagen contraction. Strong adhesion between two cell types helps maintain the sustained activation of myofibroblasts via TGF-β signaling [49]. Future studies should investigate whether integrin-mediated adhesion occurs between macrophages and fibroblasts in the myopic ciliary body, and whether this interaction triggers pro-fibrotic signaling, including Ca^{2+} influx and TGF-β activation, as reported in other fibrotic contexts. As a smooth muscle, the ciliary muscle is mainly responsible for relaxation and contraction regulation. Fukiage *et al.* [50] reported that both ROCK1 and ROCK2 mRNAs are expressed in most ocular tissues of rabbits and monkeys and that ROCK may regulate ciliary muscle contraction through phosphorylation of MLCP. Thus, we speculate that the activation of ROCK leads to contraction of actin, which is involved in smooth muscle cell contraction.

The imbalance of Ca^{2+} homeostasis is closely related to fibrotic diseases. During the development of renal fibrosis, calcium channel expression or intracellular Ca^{2+} levels are significantly increased in both *in vivo* renal tissues and *in vitro* fibroblasts, podocytes and renal tubular epithelial cells, suggesting that the abnormal regulation of intracellular Ca^{2+} is involved in the occurrence and development of renal fibrosis [51]. Orai1-dependent Ca^{2+} entry promotes atherogenesis possibly by promoting foam cell formation and vascular inflammation [52]. Cytomechanical sensation has been recognized as an indirect causative factor of fibrotic lesions [53]. Rap 1 regulates mechanical transduction by sensing mechanical stress and promoting muscle contraction or relaxation, thereby reshaping collagen fibers in the tumor interstitial environment [54,55]. The level of intracellular calcium ions is a key factor affecting cell contraction; an increase in intracellular calcium ions triggers the release of a large amount of calcium in the sarcoplasmic reticulum, resulting in an instant increase in Ca^{2+} influx, which increases contractile ability [56] and promotes the contraction of muscle fibers. Young's modulus can be used to measure the ability of a material to resist elastic deformation and thus evaluate the elastic properties of the material. Hooke's law states that within the elastic limit, the stress (σ) is proportional to the strain (ε), and the proportionality coefficient is Young's modulus (E); thus, when the mechanical stress increases, Young's modulus increases, and Ca^{2+} inflow increases. In the present study, there was an increase in Young's modulus and significant Ca^{2+} influx in the ciliary body tissue in the LIM group, indicating that the occurrence and development of myopia involve an increase in mechanical stress. The increase in Ca^{2+} concentration is an observational phenomenon related to the myopia model, but its specific interaction relationship with the ROCK pathway remains to be clarified. In addition, we plan to adopt ROCK inhibitors and Ca^{2+} channel blocking intervention to clarify whether the enhanced Ca^{2+} influx is an upstream trigger or a downstream effect of ROCK activation and further reveal the causal relationship between these two key signal nodes in myopic ciliary body remodeling.

Myofibroblasts transformed by the EMT of ciliary epithelial cells function as fibroblasts and smooth muscle cells [57]. Our previous studies revealed that retinal fibrosis is involved in the occurrence and development of myopia and that activation of the PI3K/AKT/ERK signaling pathway promotes the expression of MMP2, Col1, and α-SMA, thereby inducing retinal fibrosis [58]. In the present study, the expression levels of TGF-β1, RhoA, ROCK1, and ROCK2 in the ciliary body of guinea pigs after 2 weeks of myopia induction were significantly greater than those in the NC group, and α-SMA and Col-1 were also highly expressed. These results suggested that the enhancement of intraocular refractive regulation of ciliary body contraction in guinea pigs in the early stage of myopia promotes the activation of the TGF-β/RhoA/ROCK signaling pathway, resulting in actomyosin contraction. The expression levels of RhoA, ROCK1, ROCK2, and fibrosis-related molecules in the ciliary body of guinea pigs after 6 weeks of myopia induction continued to increase due to increased contraction. Therefore, activation of the TGF-β/RhoA/ROCK signaling pathway leads to ciliary body fibrosis and dysfunction, further inducing myopic ciliary body EMT and fibrosis (Fig. 8).

During the progression of myopia, the sclera undergoes remodeling, manifested as the degradation and rearrangement of collagen fibers, thinning of the sclera, and elongation of the eye axis. TGF-β is a key factor in maintaining collagen synthesis and tissue strength. Its reduction directly leads to a decrease in collagen (such as COL-1) synthesis and tissue thinning. TGF-β serves as a key mediator for collagen loss in the sclera of myopic eyes. Therefore, a reduction in TGF-β subtypes and a significant decrease in collagen synthesis occur in the sclera of myopic eyes [59]. The previous research results of our research team also showed that during the scleral remodeling process of lens-induced myopic guinea pigs, there was a decrease in the levels of TGF-β1, COL-1, and α-SMA [60–62], which is consistent with the previous reports of lower TGF-β1 levels in myopic sclera [63,64]. Therefore, the ciliary body does not merely convey a simple "pro-fibrotic" signal to the sclera, but rather a "pro-remodeling" or "de-stabilizing" signal. This signal leads to the disruption of scleral homeostasis, manifested as a decrease in TGF-β1 levels and the loss of collagen.

Significantly, the pathological significance of our findings is further underscored by the well-established role of the RhoA/ROCK pathway in another major ocular disease: glaucoma. ROCK inhibitors (e.g., Netarsudil, Ripasudil) are clinically approved therapeutics for glaucoma, whose primary mechanism of action is to induce relaxation of the ciliary muscle and the trabecular meshwork, thereby facilitating aqueous humor outflow and reducing intraocular pressure (IOP) [65,66]. In glaucoma, excessive ROCK activity increases the contractile tone in the outflow pathway, making its inhibition a valuable therapeutic approach. Our study indicates that in the myopic ciliary body, ROCK overactivity similarly leads to a hyper-contractile and profibrotic state, characterized by EMT, α-SMA expression, and ECM remodeling. This convergence of pathway dysregulation in two distinct ocular conditions suggests that the ciliary body is a common node of pathophysiology. It raises the intriguing hypothesis that ROCK inhibition, which is beneficial in glaucoma by relaxing the ciliary body to improve outflow, might also mitigate the fibrotic and dysfunctional changes we observed in the myopic ciliary body. Therefore, dysregulation of the TGF-β/RhoA/ROCK axis may represent a shared mechanism contributing to both high IOP in glaucoma and impaired accommodation and ocular growth in myopia. This connection significantly broadens the implications of our findings beyond myopia and positions them within a validated clinical framework.

Our research holds potential prospects for the clinical treatment of myopia. Firstly, the activation of the TGF-β/RhoA/ROCK pathway and fibrotic process occurring in the ciliary body provide a potential pathological explanation for the clinical observations of 'accommodative lag' and the difficulty in reversing myopia progression. This suggests that the onset and development of myopia involve not only passive axial elongation but also an active, pathological remodeling of anterior segment accommodation function. More importantly, our research has identified a new potential therapeutic target for intervening in the early stage of myopia, which may inhibit or slow down the progression of myopia from the source by targeting the reversal of ciliary fibrosis remodeling. It is worth noting that ROCK inhibitors have accumulated a large amount of clinical safety data in glaucoma, which may contribute to the rapid conversion pathway of "drug reuse" or the development of similar myopia control drugs. In addition, validating the effectiveness of locally administered ROCK inhibitors in animal models and exploring the use of ciliary fibrosis-related markers as indicators of myopia activity and treatment response will be crucial steps in translating these findings into clinical practice.

Our current research is not without its limitations. A significant area for future investigation is the potential reversibility of the pathological process of ciliary body fibrosis in myopic guinea pigs. To address this, we plan to introduce a recovery group comprising myopic guinea pigs. This group will undergo removal of negative lens induction at various time points throughout the development of myopic ciliary body fibrosis. Subsequently, we will assess whether there is a reduction in the levels of epithelial-mesenchymal transition (EMT) and fibrosis markers. This approach may yield valuable insights into the reversible nature of ciliary body fibrosis in the context of myopia. Due to the limitations of some advanced detection methods, such as high cost and complex technology, we use a smaller sample size (n = 3). Although this provides a clear preliminary insight, it requires careful interpretation and a larger cohort for further verification in the future. In addition, we plan to explore the deeper mechanism of inhibiting the activation of the TGF-β/RhoA/ROCK signaling pathway through drug intervention, improving the fibrosis of the ciliary body tissue, and integrating retinal results to establish a direct correlation between ciliary body fibrosis and changes in retinal morphology and function, creating new possibilities for exploring clinical treatment targets for myopia.

5. Conclusion

In summary, the activation of the TGF-β/RhoA/ROCK signaling pathway in the ciliary body in the early stage of myopia, the increase in ciliary body Ca^{2+} inflow, the increase in elastic modulus, the decrease in elasticity, and the aggravation of experimental myopic ciliary body epithelial interstitial transformation and fibrosis, accompanied by abnormal ciliary body tissue morphology in the aggravation of myopia, suggest the pathological role of the TGF-β/RhoA/ROCK signaling pathway and ciliary body fibrosis in guinea pigs with myopia. These findings will help to elucidate the molecular mechanism of myopic progression and provide new insights into myopia for clinical practice.

Availability of Data and Materials

The datasets used and analyzed during the current study are available from the corresponding author on reasonable request.

Author Contributions

XWY, YXH, and DDG designed the research study. ZYM, BB, and XWY performed the research. HXW, QXW, TLL, JWH, HSB, and XZ worked on the acquisition and organization of the experimental data information. YXX analyzed the data. All authors contributed to editorial changes in the manuscript. All authors read and approved the final manuscript. All authors have participated sufficiently in the work and agreed to be accountable for all aspects of the work.

Ethics Approval and Consent to Participate

The present study has been approved by the Ethics Committee of Affiliated Hospital of Shandong Univer-

sity of Traditional Chinese Medicine (AWE-2022-055) and strictly followed the Association for Animal Research in Vision and Ophthalmology (ARVO) principles.

Acknowledgment

Not applicable.

Funding

This work was supported by grants from the Science & Technology Project of Medicine and Health of Shandong Province (202307021591), the "Taishan Scholar" Project Special Fund (tsqnz20231252), the Youth Talent Support Program of the China Association of Chinese Medicine (2025-QNRC2-B37), the Clinical Research Project of Shandong University of Traditional Chinese Medicine (LCKY202435), the National Key R&D Program of China (2021YFC2702103), the Natural Science Foundation of Shandong Province (ZR2024MH057), the special funding from the China Postdoctoral Science Foundation (2024T170532, GZC20231505).

Conflict of Interest

The authors declare no conflict of interest.

References

[1] Bremond-Gignac D. Myopia in children. Medecine Sciences: M/S. 2020; 36: 763–768. https://doi.org/10.1051/medsci/2020131. (In French)

[2] Morgan IG, French AN, Ashby RS, Guo X, Ding X, He M, *et al*. The epidemics of myopia: Aetiology and prevention. Progress in Retinal and Eye Research. 2018; 62: 134–149. https://doi.org/10.1016/j.preteyeres.2017.09.004.

[3] Wu PC, Huang HM, Yu HJ, Fang PC, Chen CT. Epidemiology of Myopia. Asia-Pacific Journal of Ophthalmology (Philadelphia, Pa.). 2016; 5: 386–393. https://doi.org/10.1097/APO.0000000000000236.

[4] He M, Zeng J, Liu Y, Xu J, Pokharel GP, Ellwein LB. Refractive error and visual impairment in urban children in southern china. Investigative Ophthalmology & Visual Science. 2004; 45: 793–799. https://doi.org/10.1167/iovs.03-1051.

[5] Morgan IG, Wu PC, Ostrin LA, Tideman JWL, Yam JC, Lan W, *et al*. IMI Risk Factors for Myopia. Investigative Ophthalmology & Visual Science. 2021; 62: 3. https://doi.org/10.1167/iovs.62.5.3.

[6] Pucker AD, Jackson AR, McHugh KM, Mutti DO. Morphological ciliary muscle changes associated with form deprivation-induced myopia. Experimental Eye Research. 2020; 193: 107963. https://doi.org/10.1016/j.exer.2020.107963.

[7] Bailey MD, Sinnott LT, Mutti DO. Ciliary body thickness and refractive error in children. Investigative Ophthalmology & Visual Science. 2008; 49: 4353–4360. https://doi.org/10.1167/iovs.08-2008.

[8] Mutti DO, Mitchell GL, Hayes JR, Jones LA, Moeschberger ML, Cotter SA, *et al*. Accommodative lag before and after the onset of myopia. Investigative Ophthalmology & Visual Science. 2006; 47: 837–846. https://doi.org/10.1167/iovs.05-0888.

[9] Weinreb RN, Lindsey JD, Luo XX, Wang TH. Extracellular matrix of the human ciliary muscle. Journal of Glaucoma. 1994; 3: 70–78.

[10] Zeisberg M, Kalluri R. Cellular mechanisms of tissue fibrosis. 1. Common and organ-specific mechanisms associated with tissue fibrosis. American Journal of Physiology. Cell Physiology. 2013; 304: C216–C225. https://doi.org/10.1152/ajpcell.00328.2012.

[11] Wu H, Yu Y, Huang H, Hu Y, Fu S, Wang Z, *et al*. Progressive pulmonary fibrosis is caused by elevated mechanical tension on alveolar stem cells. Cell. 2021; 184: 845–846. https://doi.org/10.1016/j.cell.2021.01.020.

[12] Yamanaka O, Liu CY, Kao WWY. Fibrosis in the anterior segments of the eye. Endocrine, Metabolic & Immune Disorders Drug Targets. 2010; 10: 331–335. https://doi.org/10.2174/1871530311006040331.

[13] Greene W, Burke T, Bramblett G, Wang HC. Detection of Retinal Fibrosis in a Rabbit Model of Penetrating Eye Injury. Military Medicine. 2020; 185: 443–447. https://doi.org/10.1093/milmed/usz221.

[14] Milivojević M, Vukosavljević M, Aleksić P, Stojković R, Dimitrijević J, Latković Z, *et al*. Comparison of the suppressing capecitabine and 5-fluorouracil effects on the pronounce of inflammatory cells score in the induction of episcleral fibrosis after trabeculectomy. Vojnosanitetski Pregled. 2007; 64: 449–452. https://doi.org/10.2298/vsp0707449m. (In Serbian)

[15] Zhang Z, Liu X, Shen Z, Quan J, Lin C, Li X, *et al*. Endostatin in fibrosis and as a potential candidate of anti-fibrotic therapy. Drug Delivery. 2021; 28: 2051–2061. https://doi.org/10.1080/10717544.2021.1983071.

[16] Thiery JP, Acloque H, Huang RYJ, Nieto MA. Epithelial-mesenchymal transitions in development and disease. Cell. 2009; 139: 871–890. https://doi.org/10.1016/j.cell.2009.11.007.

[17] Iwano M, Plieth D, Danoff TM, Xue C, Okada H, Neilson EG. Evidence that fibroblasts derive from epithelium during tissue fibrosis. The Journal of Clinical Investigation. 2002; 110: 341–350. https://doi.org/10.1172/JCI15518.

[18] Lamouille S, Xu J, Derynck R. Molecular mechanisms of epithelial-mesenchymal transition. Nature Reviews. Molecular Cell Biology. 2014; 15: 178–196. https://doi.org/10.1038/nrm3758.

[19] Biernacka A, Dobaczewski M, Frangogiannis NG. TGF-β signaling in fibrosis. Growth Factors (Chur, Switzerland). 2011; 29: 196–202. https://doi.org/10.3109/08977194.2011.595714.

[20] Zhang K, Zhang H, Xiang H, Liu J, Liu Y, Zhang X, *et al*. TGF-β1 induces the dissolution of tight junctions in human renal proximal tubular cells: role of the RhoA/ROCK signaling pathway. International Journal of Molecular Medicine. 2013; 32: 464–468. https://doi.org/10.3892/ijmm.2013.1396.

[21] Zhou X, Qu J, Xie R, Wang R, Jiang L, Zhao H, *et al*. Normal development of refractive state and ocular dimensions in guinea pigs. Vision Research. 2006; 46: 2815–2823. https://doi.org/10.1016/j.visres.2006.01.027.

[22] Baird PN, Saw SM, Lanca C, Guggenheim JA, Smith Iii EL, Zhou X, *et al*. Myopia. Nature Reviews. Disease Primers. 2020; 6: 99. https://doi.org/10.1038/s41572-020-00231-4.

[23] Holden BA, Fricke TR, Wilson DA, Jong M, Naidoo KS, Sankaridurg P, *et al*. Global Prevalence of Myopia and High Myopia and Temporal Trends from 2000 through 2050. Ophthalmology. 2016; 123: 1036–1042. https://doi.org/10.1016/j.ophtha.2016.01.006.

[24] Jeon S, Lee WK, Lee K, Moon NJ. Diminished ciliary muscle movement on accommodation in myopia. Experimental Eye Research. 2012; 105: 9–14. https://doi.org/10.1016/j.exer.2012.08.014.

[25] Tamm E, Lütjen-Drecoll E, Jungkunz W, Rohen JW. Posterior attachment of ciliary muscle in young, accommodating old, presbyopic monkeys. Investigative Ophthalmology & Visual Science. 1991; 32: 1678–1692.

[26] Chen Y, Gao J, Li L, Sellitto C, Mathias RT, Donaldson PJ, *et al*. The Ciliary Muscle and Zonules of Zinn Modulate Lens In-

tracellular Hydrostatic Pressure Through Transient Receptor Potential Vanilloid Channels. Investigative Ophthalmology & Visual Science. 2019; 60: 4416–4424. https://doi.org/10.1167/iovs.19-27794.

[27] Fernández-Vigo JI, Kudsieh B, Shi H, De-Pablo-Gómez-de-Liaño L, Fernández-Vigo JÁ, García-Feijóo J. Diagnostic imaging of the ciliary body: Technologies, outcomes, and future perspectives. European Journal of Ophthalmology. 2022; 32: 75–88. https://doi.org/10.1177/11206721211031409.

[28] Branton MH, Kopp JB. TGF-beta and fibrosis. Microbes and Infection. 1999; 1: 1349–1365. https://doi.org/10.1016/s1286-4579(99)00250-6.

[29] Ji H, Tang H, Lin H, Mao J, Gao L, Liu J, *et al*. Rho/Rock cross-talks with transforming growth factor-β/Smad pathway participates in lung fibroblast-myofibroblast differentiation. Biomedical Reports. 2014; 2: 787–792. https://doi.org/10.3892/br.2014.323.

[30] Darby IA, Hewitson TD. Fibroblast differentiation in wound healing and fibrosis. International Review of Cytology. 2007; 257: 143–179. https://doi.org/10.1016/S0074-7696(07)57004-X.

[31] Veres-Székely A, Pap D, Szikszi E, Jávorszky E, Rokonay R, Lippai R, *et al*. Selective measurement of α smooth muscle actin: why β-actin can not be used as a housekeeping gene when tissue fibrosis occurs. BMC Molecular Biology. 2017; 18: 12. https://doi.org/10.1186/s12867-017-0089-9.

[32] Coward WR, Saini G, Jenkins G. The pathogenesis of idiopathic pulmonary fibrosis. Therapeutic Advances in Respiratory Disease. 2010; 4: 367–388. https://doi.org/10.1177/1753465810379801.

[33] Wynn TA. Integrating mechanisms of pulmonary fibrosis. The Journal of Experimental Medicine. 2011; 208: 1339–1350. https://doi.org/10.1084/jem.20110551.

[34] Korol A, Taiyab A, West-Mays JA. RhoA/ROCK signaling regulates TGFβ-induced epithelial-mesenchymal transition of lens epithelial cells through MRTF-A. Molecular Medicine (Cambridge, Mass.). 2016; 22: 713–723. https://doi.org/10.2119/molmed.2016.00041.

[35] Kerrigan JJ, Mansell JP, Sandy JR. Matrix turnover. Journal of Orthodontics. 2000; 27: 227–233. https://doi.org/10.1179/orth.o.27.3.227.

[36] Egeblad M, Werb Z. New functions for the matrix metalloproteinases in cancer progression. Nature Reviews. Cancer. 2002; 2: 161–174. https://doi.org/10.1038/nrc745.

[37] Ziober BL, Turner MA, Palefsky JM, Banda MJ, Kramer RH. Type I collagen degradation by invasive oral squamous cell carcinoma. Oral Oncology. 2000; 36: 365–372. https://doi.org/10.1016/s1368-8375(00)00019-1.

[38] Brinckerhoff CE, Rutter JL, Benbow U. Interstitial collagenases as markers of tumor progression. Clinical Cancer Research: an Official Journal of the American Association for Cancer Research. 2000; 6: 4823–4830.

[39] Arakaki PA, Marques MR, Santos MCLG. MMP-1 polymorphism and its relationship to pathological processes. Journal of Biosciences. 2009; 34: 313–320. https://doi.org/10.1007/s12038-009-0035-1.

[40] Wang CH, Lin HC, Lin SM, Huang CD, Liu CY, Huang KH, *et al*. MMP-1(-1607G) polymorphism as a risk factor for fibrosis after pulmonary tuberculosis in Taiwan. The International Journal of Tuberculosis and Lung Disease: the Official Journal of the International Union against Tuberculosis and Lung Disease. 2010; 14: 627–634.

[41] Bhowmick NA, Ghiassi M, Bakin A, Aakre M, Lundquist CA, Engel ME, *et al*. Transforming growth factor-beta1 mediates epithelial to mesenchymal transdifferentiation through a RhoA-dependent mechanism. Molecular Biology of the Cell. 2001; 12: 27–36. https://doi.org/10.1091/mbc.12.1.27.

[42] Masszi A, Di Ciano C, Sirokmány G, Arthur WT, Rotstein OD, Wang J, *et al*. Central role for Rho in TGF-beta1-induced alpha-smooth muscle actin expression during epithelial-mesenchymal transition. American Journal of Physiology. Renal Physiology. 2003; 284: F911–F924. https://doi.org/10.1152/ajprenal.00183.2002.

[43] Miesfeld JB, Brown NL. Eye organogenesis: A hierarchical view of ocular development. Current Topics in Developmental Biology. 2019; 132: 351–393. https://doi.org/10.1016/bs.ctdb.2018.12.008.

[44] Torregrossa M, Davies L, Hans-Günther M, Simon JC, Franz S, Rinkevich Y. Effects of embryonic origin, tissue cues and pathological signals on fibroblast diversity in humans. Nature Cell Biology. 2025; 27: 720–735. https://doi.org/10.1038/s41556-025-01638-5.

[45] Lujano Olazaba O, Farrow J, Monkkonen T. Fibroblast heterogeneity and functions: insights from single-cell sequencing in wound healing, breast cancer, ovarian cancer and melanoma. Frontiers in Genetics. 2024; 15: 1304853. https://doi.org/10.3389/fgene.2024.1304853.

[46] Younesi FS, Miller AE, Barker TH, Rossi FMV, Hinz B. Fibroblast and myofibroblast activation in normal tissue repair and fibrosis. Nature Reviews. Molecular Cell Biology. 2024; 25: 617–638. https://doi.org/10.1038/s41580-024-00716-0.

[47] Ma F, Tsou PS, Gharaee-Kermani M, Plazyo O, Xing X, Kirma J, *et al*. Systems-based identification of the Hippo pathway for promoting fibrotic mesenchymal differentiation in systemic sclerosis. Nature Communications. 2024; 15: 210. https://doi.org/10.1038/s41467-023-44645-6.

[48] Hinz B, Lagares D. Evasion of apoptosis by myofibroblasts: a hallmark of fibrotic diseases. Nature Reviews. Rheumatology. 2020; 16: 11–31. https://doi.org/10.1038/s41584-019-0324-5.

[49] Ezzo M, Spindler K, Wang JB, Lee D, Pecoraro G, Cowen J, *et al*. Acute contact with profibrotic macrophages mechanically activates fibroblasts via αvβ3 integrin-mediated engagement of Piezo1. Science Advances. 2024; 10: eadp4726. https://doi.org/10.1126/sciadv.adp4726.

[50] Fukiage C, Mizutani K, Kawamoto Y, Azuma M, Shearer TR. Involvement of phosphorylation of myosin phosphatase by ROCK in trabecular meshwork and ciliary muscle contraction. Biochemical and Biophysical Research Communications. 2001; 288: 296–300. https://doi.org/10.1006/bbrc.2001.5751.

[51] Mai X, Shang J, Liang S, Yu B, Yuan J, Lin Y, *et al*. Blockade of Orai1 Store-Operated Calcium Entry Protects against Renal Fibrosis. Journal of the American Society of Nephrology: JASN. 2016; 27: 3063–3078. https://doi.org/10.1681/ASN.2015080889.

[52] Liang SJ, Zeng DY, Mai XY, Shang JY, Wu QQ, Yuan JN, *et al*. Inhibition of Orai1 Store-Operated Calcium Channel Prevents Foam Cell Formation and Atherosclerosis. Arteriosclerosis, Thrombosis, and Vascular Biology. 2016; 36: 618–628. https://doi.org/10.1161/ATVBAHA.116.307344.

[53] Long Y, Niu Y, Liang K, Du Y. Mechanical communication in fibrosis progression. Trends in Cell Biology. 2022; 32: 70–90. https://doi.org/10.1016/j.tcb.2021.10.002.

[54] Bayer SV, Grither WR, Brenot A, Hwang PY, Barcus CE, Ernst M, *et al*. DDR2 controls breast tumor stiffness and metastasis by regulating integrin mediated mechanotransduction in CAFs. eLife. 2019; 8: e45508. https://doi.org/10.7554/eLife.45508.

[55] Kosuru R, Chrzanowska M. Integration of Rap1 and Calcium Signaling. International Journal of Molecular Sciences. 2020; 21: 1616. https://doi.org/10.3390/ijms21051616.

[56] Zhang HZ, Cui CC, Zhao XJ, Du KX, Liu J. Response to calcium of effects of electric stimulations applied during absolute refractory period on the contractility of ventricular muscle in rabbits.

Journal of Xi'an Jiaotong University (Medical Edition). 2003; 318–320. (In Chinese)

[57] Phan SH. Genesis of the myofibroblast in lung injury and fibrosis. Proceedings of the American Thoracic Society. 2012; 9: 148–152. https://doi.org/10.1513/pats.201201-011AW.

[58] Bao B, Liu J, Li T, Yang Z, Wang G, Xin J, *et al*. Elevated retinal fibrosis in experimental myopia is involved in the activation of the PI3K/AKT/ERK signaling pathway. Archives of Biochemistry and Biophysics. 2023; 743: 109663. https://doi.org/10.1016/j.abb.2023.109663.

[59] McBrien NA. Regulation of scleral metabolism in myopia and the role of transforming growth factor-beta. Experimental Eye Research. 2013; 114: 128–140. https://doi.org/10.1016/j.exer.2013.01.014.

[60] Zhang R, Wen Y, Liu J, Hao J, Peng Y, Zhang M, *et al*. The miR-15b-5p/miR-379-3p-FOXO axis regulates cell cycle and apoptosis in scleral remodeling during experimental myopia. Journal of Translational Medicine. 2024; 22: 710. https://doi.org/10.1186/s12967-024-05523-x.

[61] Li X, Liu X, Yu Y, Li T, Guo L, Hu G, *et al*. Covariation of scleral remodeling and PI3K/Akt signaling pathway in experimental myopia. Scientific Reports. 2025; 15: 12476. https://doi.org/10.1038/s41598-025-97643-7.

[62] Zhang M, Zhang R, Hao J, Zhao X, Ma Z, Peng Y, *et al*. Quercetin Alleviates Scleral Remodeling Through Inhibiting the PERK-EIF2α Axis in Experiment Myopia. Investigative Ophthalmology & Visual Science. 2024; 65: 11. https://doi.org/10.1167/iovs.65.13.11.

[63] Li M, Yuan Y, Chen Q, Me R, Gu Q, Yu Y, *et al*. Expression of Wnt/β-Catenin Signaling Pathway and Its Regulatory Role in Type I Collagen with TGF-β1 in Scleral Fibroblasts from an Experimentally Induced Myopia Guinea Pig Model. Journal of Ophthalmology. 2016; 2016: 5126560. https://doi.org/10.1155/2016/5126560.

[64] Guo L, Frost MR, Siegwart JT, Jr, Norton TT. Scleral gene expression during recovery from myopia compared with expression during myopia development in tree shrew. Molecular Vision. 2014; 20: 1643–1659.

[65] Schehlein EM, Robin AL. Rho-Associated Kinase Inhibitors: Evolving Strategies in Glaucoma Treatment. Drugs. 2019; 79: 1031–1036. https://doi.org/10.1007/s40265-019-01130-z.

[66] Wang R, Wei H, Shi Y, Wang C, Yu Z, Zhang Y, *et al*. Self-generating electricity system driven by aqueous humor flow and trabecular meshwork contraction motion activated BCKa for glaucoma intraocular pressure treatment. Materials Horizons. 2025; 12: 434–450. https://doi.org/10.1039/d4mh01004c.